Landslide Susceptibility Assessment Tools v1.0.0b - Project Manager Suite: A new modular toolkit for landslide susceptibility assessment.

Jewgenij Torizin[1], Nick Schüßler[1], Michael Fuchs[1]

5   [1]Federal Institute for Geosciences and Natural Resources (BGR), Hanover, 30655, Germany

Correspondence to: Jewgenij Torizin (jewgenij.torizin@bgr.de)

Abstract. This paper introduces the Landslide Susceptibility Assessment Tools – Project Manager Suite (LSAT PM), an open-source, easy-to-use software written in Python. Primarily developed to conduct landslide susceptibility analyses (LSA), it is not limited to this issue and applies to any other research dealing with supervised spatial binary classification. LSAT PM

10   provides efficient interactive data management supported by handy tools in a standardized project framework. The application utilizes open standard data formats ensuring data transferability to all geographic information systems. LSAT PM has a modular structure that allows extending the existing toolkit by additional tools. The LSAT PM v1.0.0b implements heuristic and data-driven methods: analytical hierarchy process, weights of evidence, logistic regression, and artificial neural networks. The software was developed and tested over the years in different projects dealing with landslide susceptibility assessment.

15   The emphasis on model uncertainties and statistical model evaluation makes the software a practical modeling tool to explore and evaluate different native and foreign LSA models. The software distribution package includes comprehensive documentation. A dataset for testing purposes of the software is available. LSAT PM is subject to continuous further development.

1 Introduction

20   Landslides occur in all mountainous parts of the world, significantly contributing to disastrous socio-economic consequences and claiming thousands of casualties every year (Petley, 2012; Froude and Petley, 2018). These phenomena are frequently associated with other natural hazards such as severe rainfalls, floods, and earthquakes (e.g., Polemio and Petrucci, 2000; Crozier, 2010; Keefer, 2002; Kamp et al., 2008).

Per definition, a comprehensive assessment of landslide hazards addresses the spatial and temporal landslide occurrence based

25   on three questions: "Where?", "When?" and "How large?" (e.g., Varnes, 1984, Guzzetti et al., 1999, Tanyaş et al., 2018; Reichenbach et al., 2018). The landslide susceptibility analysis (LSA) depicts the probability of spatial landslide occurrence (e.g., Brabb, 1985; Guzzetti et al., 2005) covering the spatial domain of the hazard analysis. Addressing the temporal domain of landslide hazard assessment is much more challenging due to the local character of the phenomenon and a common lack of multi-temporal landslide inventories covering sufficient periods (e.g., Aleotti and Chowdhury, 1999; Van Westen et al., 2006).

30   Therefore, most case studies at regional scales focus on LSA as the most feasible part of the landslide hazard analysis.

Regional LSA is usually done based on qualitative (heuristic or knowledge-driven) and quantitative methods (e.g., Reichenbach et al. 2018). The quantitative techniques comprise physically-based and data-driven statistical and machine learning (ML) approaches (e.g., Aleotti and Chowdhury, 1999). The desired analysis scale and data availability usually govern the decision of which method to use (e.g., Van Westen et al., 2008; Balzer et al., 2020).

35 In the past decades, advances in remote sensing made significant progress allowing efficient data acquisition at regional scales. Additionally, digitalization forced a general boost of data mining techniques. Together with the development of GIS software packages and open-source statistical and machine learning libraries, the data-driven methods for LSA have gained popularity. These methods belong mainly to supervised binary classification (e.g., Torizin, 2016). In the supervised classification, we use a set of recorded observations (labels) and independent explanatory factors (features) such as different geomorphologic,

40 hydrologic, and geological conditions to train a statistic function (classifier). The classifier estimates the likelihood of a specific countable element in a study area (e.g., raster pixel) to be in the specified target class (e.g., landslide or no landslide).

Because classification is one of the fundamental tasks in statistics and ML, many different classifiers exist. Consequently, in numerous case studies, the academic community continuously applies and compares classification algorithms and their variations, which were initially developed for other purposes but are sufficiently general to be used for LSA. While some

45 classifiers might outperform others, the drawn conclusions are often valid only for particular settings and study designs (e.g., Balzer et al., 2020). Under other circumstances, such as different data quality or distribution, it is very likely that some of the other classifiers perform on par or better. Reviewing the LSA research of the past 30 years, Reichenbach et al. (2018) counted about 163 different data-driven methods, emphasizing the problem of excessive experimentation with statistical classifiers rather than focusing on the LSA's reliability. Many of these methods have never been adopted or seriously considered by

50 practitioners skeptically following the academic research at their own pace and utilizing a comparably small part of it. Thus, despite the many academic publications dealing with regional data-driven LSA, only a few practical solutions have been adopted in national landslide risk assessment strategies yet (e.g., Balzer et al., 2020). Also, user-friendly standalone software developed in this field is rare compared to the available geotechnical software applications. Many available tools exist as academic code generated to support specific case studies (e.g., Merghadi, 2018; Merghadi, 2019; GitHub, 2021a; GitHub,

55 2021b) and imply that the user has the necessary programming or scripting skills to set up and run the tools. Despite considerable efforts to adopt the earth science curricula to digital transformation (e.g., Hall-Wallace, 1999; Makkawi et al., 2006, Senger et al., 2021), the required computational literacy to deal with those applications is not a broad standard in geosciences. However, there is a positive trend. Rising education possibilities on e-learning platforms with exhaustive offers in programming narrow the gap between geosciences and data sciences. Bouziat et al. (2020) noted that the geoscience

60 community increasingly uses Python (Van Rossum & Drake, 2009) for data processing, R statistical package (R Core Team, 2013) for statistical analysis, and custom web services for sharing results.

Since 2010, many LSA tools have been available as plugins or extensions in different GIS such as, e.g., LSAT (Polat, 2021), LSM Tool Pack (Sahin et al., 2020), or ArcMAP Tool (Jebur et al., 2015) in ESRI ArcGIS, SZ-plugin (Titti & Sarretta, 2020) in QGIS (QGIS Development Team, 2009), r.landslide (Bragagnolo et al., 2020a) in GRASS GIS (GRASS Development

65   Team, 2021), and RSAGA (Brenning, 2008) in SAGA, as well as scripts in R statistical package, e.g., LAND-SE (Rossi and
      Reichenbach, 2016), and very few standalone applications, e.g., GeoFIS (Osna et al., 2014).

      With the Landslide Susceptibility Assessment Tools – Project Manager Suite (LSAT PM), we introduce an open-source (GNU
      General Public License v3), standalone and easy-to-use tool that supports scientific principles of openness, knowledge
      integrity, and replicability. Doing so, we want to share our experience in implementing heuristic and data-driven LSA methods.

70   Our primary goal is not to introduce as many algorithms as possible for LSA but to provide easy access to a selection of state-
      of-the-art methods representing groups of different approaches. Providing a convenient framework for model building,
      evaluation, and uncertainty assessment, we want to highlight the capabilities and limitations of those methods.

2 LSAT PM Software

      LSAT PM is a desktop application designed to support decision-makers and the scientific community in generating and
75   evaluating landslide susceptibility models based on heuristic and data-driven approaches.

2.1 Development history

      The development of Landslide Susceptibility Assessment Tools (LSAT) started in 2011 with Python scripting within ESRI
      ArcGIS 10.0 Toolbox to support technical cooperation (TC) projects (Torizin, 2012). TC projects are usually not cutting-edge
      research but summarise, adapt, and implement scientific outcomes by following the best-practice approach. Since then, LSAT
80   was continuously improved and tested at different development stages in case studies in Indonesia (Torizin et al., 2013),
      Thailand (Teerarungsigul et al., 2015), Pakistan (Torizin et al., 2017), China (Torizin et al., 2018) and Germany (Balzer et al.,
      2020). Working with different data of varying quality helped us develop efficient methodical workflows. It also enabled us to
      better understand the limitations of some methods and design practical approaches to assess model uncertainties (e.g., Torizin
      et al., 2021).

85   In 2017, we started to prototype LSAT as a standalone application bearing the extension "Project Manager Suite" in Python 2
      and later in Python 3. This development began within the sino-german scientific cooperation project (Tian et al., 2017) and
      continued in a cooperation project with german geological surveys (Balzer et al., 2020).

2.2 Software architecture and capabilities

      LSAT PM v1.0.0b is written in Python 3. Graphical framework PyQt5 provides the basis for the graphical user interface (GUI).
90   Functionalities of the software rely on different third-party libraries and Python packages. Geospatial Data Abstraction
      software Library (GDAL) (GDAL/OGR Contributors, 2021) and its Python bindings provide the core functionality for dealing
      with spatial data. The highly efficient *NumPy* (Harris et al., 2020) provides array computations through the analyses.
      Implemented ML algorithms rely on the powerful *sklearn* library (Pedregosa et al., 2011; Buitinck et al., 2013). *Matplotlib*

(Hunter, 2007) provides the basis for generating analysis plots. *Openpyxl* (Gazoni and Clark, 2018) and *python-docx* (Canny, 2018) packages allow the export of analysis results as convenient MS Office files and automatized analysis reports generation. The software consists of the main GUI with integrated independent modules (widgets), building the software's functionality. Due to the LSAT PM development history, we built the most functionalities around the weights of evidence (WoE) method, which was the initial analysis module of LSAT PM. WoE (e.g., Bonham-Carter et al., 1989) belongs to the bivariate statistical methods frequently applied in LSA in the past decades (e.g., Mathew et al., 2007; Moghaddam et al., 2007; Thiery et al., 2007; Neuhäuser et al., 2012; Teerarungsigul et al., 2015). It is simple to understand and provides a transparent computation algorithm. With enhanced uncertainty assessment (e.g., Torizin et al., 2018; Torizin et al., 2021), WoE becomes a robust tool for rapid analysis providing a good reference model to test against when exploring new methods. For example, it can be beneficial to investigate the data dependencies or run several sensitivity analyses based on transparent WoE before applying more sophisticated multivariate statistical analysis techniques, e.g., logistic regression (LR) or *black-box* ML algorithms such as artificial neural networks (ANN). LSAT PM includes both LR (e.g., Lee, 2005; Budimir et al., 2015; Lombardo and Mai, 2018) and ANN (e.g., Lee and Evangelista, 2006; Pradhan and Lee, 2010; Bragagnolo et al., 2020b), and also a module for heuristic analyses based on the analytical hierarchy process (AHP). This decision support method finds application primarily for areas with insufficient observational data (e.g., Balzer et al., 2020; Panchal and Shrivastava, 2020).

Currently, LSAT PM can utilize Tagged Image File Format (GeoTiff) raster data for model parameters and vector data formats such as ESRI shapefiles, Keyhole Markup Language (KML), and JavaScript Object Notation (GeoJSON) for inventories. Further GDAL-supported formats are incorporable on demand.

Complementary to the spatial data output in the same formats as input, LSAT PM supports exporting tables to Microsoft Excel-Sheets, graphs to portable network graphic files (PNG), and automated analysis reports to MS Word documents.

For spatial analysis, LSAT PM implements basic geoprocessing functionalities for data preparation. Morphological analyses, such as slope, aspect, topographic position index (TPI), and many others, can be performed based on raster datasets in GeoTiff format. Functions such as euclidean distance and raster classification are also available. A simple data viewer visualizes raster data.

However, although LSAT PM provides some GIS capabilities for geoprocessing, it cannot be characterized as a solid GIS application and was never supposed to become one. It has a slim structure tailored to manage and prepare the data for binary spatial classification.

3 Working with LSAT PM

LSAT PM provides handy tools to set up the model through data exploration, preprocessing, analysis, model evaluation, and postprocessing.

The logical workflow in Fig. 1 schematically sketches the working process with LSAT PM. The following sections briefly
125 introduce the single steps of this workflow and their corresponding modules. More technical details are obtainable from the
software documentation distributed standalone or as part of the installer package (see also Sect. 7).
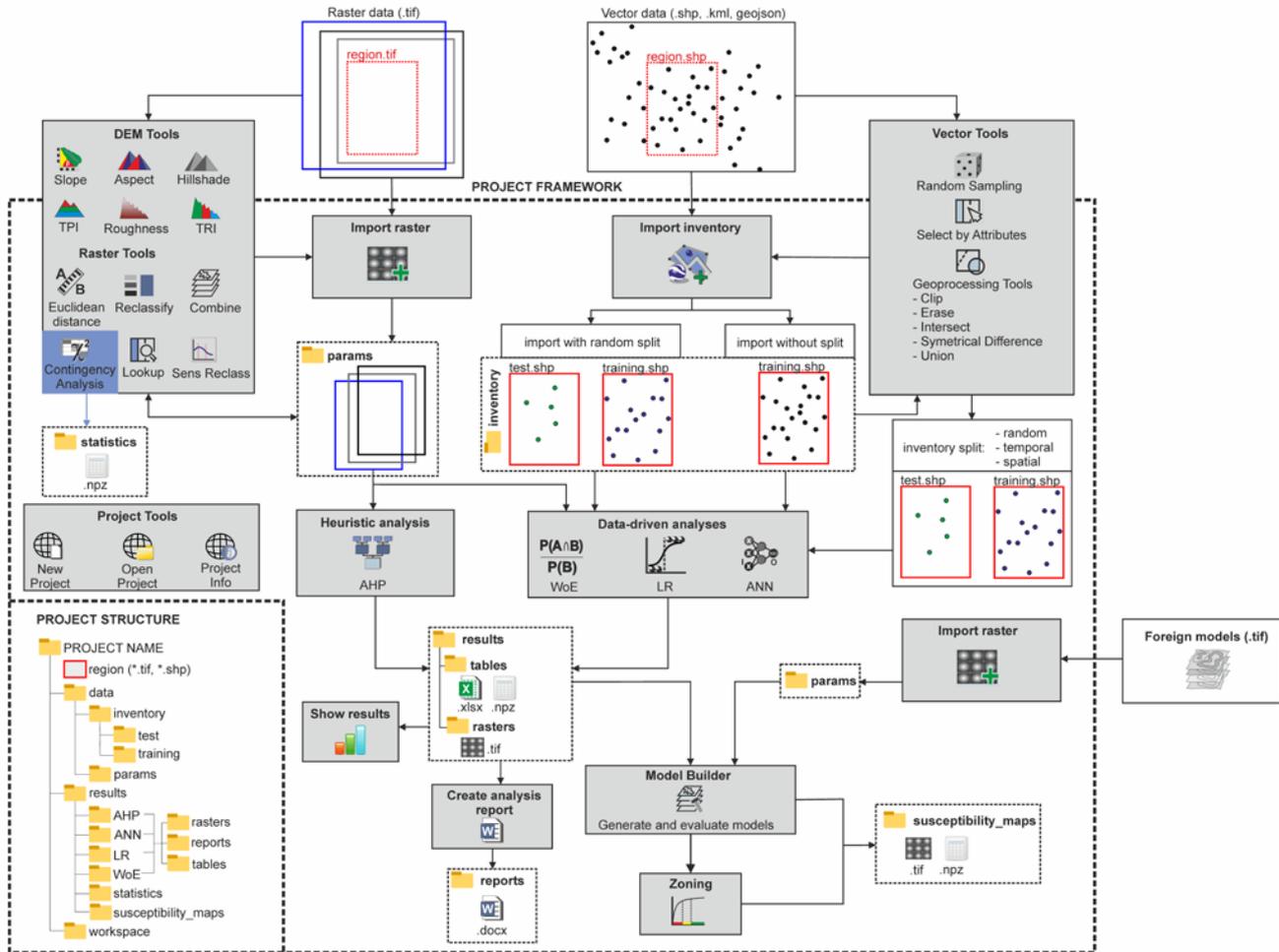
Figure 1: Standardized project structure and the logical workflow of LSAT PM.

3.1 Project

130 After launching the software, the user can create a new or open an existing project. A project is a structured folder system that
stores data with a specified spatial extent and spatial reference (region). The spatial extent and spatial reference need to be
assigned on project creation manually or by selecting an already existing raster dataset as a project reference file
(recommended).

The LSAT PM project has a standardized predefined structure, as shown in the bottom left of Fig. 1. The local project files
135 overview (*Catalog* in Fig. 2) in the main GUI helps manage the project data providing a data-type dependent context menu.

3.2 Data import

Data import distinguishes between *Import Raster* and *Import Inventory* (Fig. 2). The first tool imports raster datasets considered to represent independent exploratory factors (features), the second imports vector-based datasets for observational data representing inventory or labels.

140   The raster import tool ensures consistency by validating imported datasets against the project reference dataset (region). If not consistent with the project reference, the data gets warped. This procedure is comparable to the concept of regions found in GRASS GIS and helps avoid processing errors due to specific resolution and spatial reference inconsistencies. The import procedure generates data copies; thus, original files remain unchanged.

Inventory import generally does the same for vector datasets as input. Additionally, it includes the random splitting of the

145   dataset into training and test datasets. Using this option, the user can specify the percentage ratio of training and test datasets. The splitting option is not mandatory and skippable because inventory subsetting is possible later using one of the tools described in Sect. 3.3 (see also Fig. 1).
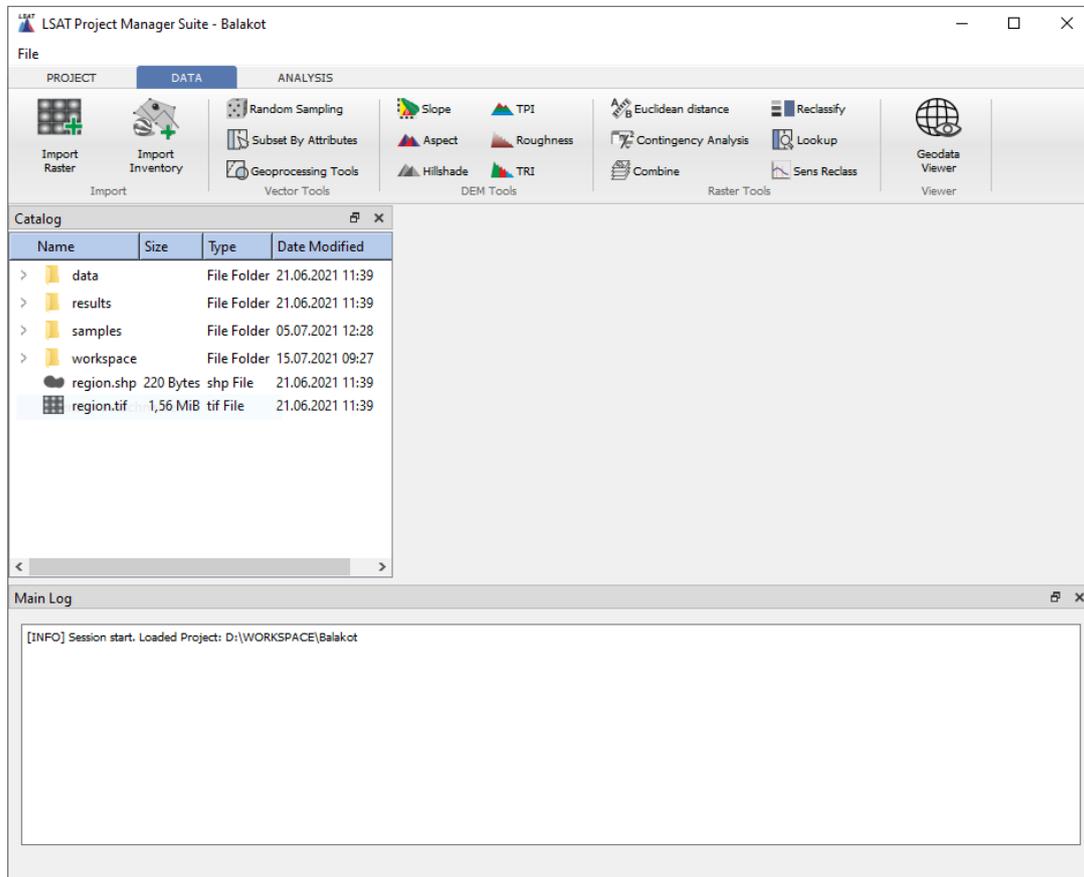
Figure 2: Main GUI with activated *Data* tab. The *Data* tab contains tools for data import, vector data processing, DEM tools, tools
150   **for raster processing, and a simple data viewer.**

3.3 Data exploration and preprocessing

In the preprocessing step, we derive parameters and prepare the data according to the requirements of the upcoming analysis. *Vector*, *DEM*, and *Raster Tools* of LSAT PM (Fig. 2) aid this purpose.

Data subsetting is an essential technique to evaluate data-driven models using a test dataset not involved in the model's training,
155 also known as cross-validation (e.g., Xu and Goodacre, 2018; Petschko et al., 2014; Chung and Fabbri, 2008). LSAT PM provides a palette of *Vector Tools* (Fig. 2) that supports the generation of inventory subsets based on random subsampling or feature attributes, e.g., the date (temporal split). Using *Geoprocessing Tools* in the same tool domain, the user can also subset the inventory based on spatial features (spatial split).

Digital elevation models (DEM) serve as a basis for morphometric parameters such as, e.g., slope, aspect, or TPI. *DEM Tools*
160 (Fig. 2) derive basic morphometric features and generate raster data outputs from DEM raster datasets.

Raster Tools help perform basic raster operations and spatial analyses. Using the *Combine* tool, the user can combine several discrete raster datasets to generate a new raster dataset exhibiting unique conditions of higher complexity. Linear and point vector data (e.g., tectonic features, roads, streams, or point locations) are usually unsuitable as direct input for spatial analysis. However, their possible spatial effects are considerable via distance maps. The *Euclidean distance* tool generates a distance
165 raster dataset based on input vector data.

Raster reclassification is a standard procedure in GIS analyses applied as value replacement in discrete datasets or binning of continuous datasets. Because WoE utilizes discrete data only, continuous raster data such as slope or distance rasters need a binning in the data preparation process. The *Reclassify* tool offers different classifiers such as equal intervals, quantiles, defined intervals, and user-defined values. Additionally, the *Sensitivity Reclassification (Sens Reclass)* tool provides a sensitivity
170 analysis to find optimal cutoff thresholds (e.g., Torizin et al., 2017).

The *Contingency Analysis* tool performs the Chi-square-based contingency analysis on raster-based categorical data, estimating the associations between the datasets based on Pearsons C, Cramer's V, and Phi. It is the only tool that produces output in the subfolder *statistics* of the projects' results folder. The user can view the output contingency table via the *Show results* option from the *Catalog's* context menu.

175 All the above-presented tools apply to datasets in any location. Thus, the user can perform preprocessing steps before the data import.

3.4 Analyses

As already introduced in Sect. 2, LSAT PM implements heuristic and data-driven methods for LSA representing different categories (e.g., bivariate and multivariate). All of the methods have different levels of complexity, which need to be accounted
180 for when choosing a specific analysis method. Table 3 briefly summarizes the corner points of the approaches such as category, supported data types, and complexity. The introduced complexity is a subjective measure that we assigned based on our experience evaluating criteria such as needed mathematical background, the complexity of data preparation, model structure

and computation algorithm (transparency), and interpretability of the results. Due to the high degree of automation, the more complex methods allow running the analysis with its default settings without any adjustment and, therefore, might appear more straightforward. However, this first impression will vanish once the user encounters the advanced settings of the methods.

Table 1 Analyses included in LSAT PM and their specifications

Analysis name	Category	Supported data types	Complexity
Weights of Evidence	data-driven, bivariate	discrete	moderate
Logistic regression	data-driven, multivariate	continuous, discrete	high
Artificial Neural Network	data-driven, multivariate	continuous, discrete	very high
Analytic Hierarchy Process	heuristic	discrete	low

3.4.1 Weights of Evidence

WoE is a bivariate statistical approach estimating the association between the observational data (dependent variable represented by the training landslide inventory) and a potential controlling factor (independent variable represented by, e.g., geological conditions). The analysis output is a raster of the specific controlling factor containing logarithmic log-likelihood weights, which characterize the relationship of discrete factor classes with a landslide occurrence. Individually weighted factors are then overlaid into a linear model to obtain the overall landslide susceptibility pattern (Torizin et al., 2017).

WoE in LSAT PM offers three different analysis modes: simple cross-validation, on-the-fly subsampling, and sampling with predefined samples. The default option is simple cross-validation (presupposes inventory split into training and test datasets). With this option, the model weights estimation runs once with the entire training dataset (no further subsampling). For on-the-fly subsampling, the weight estimation runs for several user-defined iterations taking random samples (without replacement) of user-defined size from the training inventory. The estimated weights are mean values from all iterations. The analysis with predefined samples utilizes predefined sample datasets in a specified folder location. These predefined samples must be created beforehand by any subsetting algorithm introduced above (Sect 3.3). The computed weights are mean values from all iterations, identical to the random subsampling.

After the training, the result table and the weighted raster are automatically exported into the corresponding result folders. The results can be visualized immediately after the analysis through the WoE widget or later by calling the result viewer from the *Catalog's* context menu.

The model generation process is performed in the next step using the LSAT PM model builder module (see Sect. 3.5).

3.4.2 Logistic regression

Logistic regression (LR) is a multivariate statistical classification method to estimate relationships between the dependent variable and independent controlling factors. In contrast to WoE, LR analyzes the associations for all controlling factors at once and can utilize both continuous and discrete data as independent variables.

210 In LSAT PM, LR runs more automated than WoE. The user has to determine if the parameter is a discrete or continuous variable in the beginning. After that, the data preparation process runs automatically. The continuous datasets are scaled using a min-max-scaler to the value range between 0 and 1; discrete datasets are transformed into binary dummy variables. All setting options for the logistic regression, e.g., regularisation or solver algorithm, implemented in the *sklearn* library, are adjustable upon the user's needs in the advanced settings GUI. After the training, the result table and the prediction raster are

215 automatically exported into the corresponding result folders.

Unlike WoE, the analysis output from multivariate LR already provides a multi-parameter landslide susceptibility model.

3.4.3 Artificial Neural Network

ANNs are computer models inspired by biological neural networks. They consist of artificial neurons ordered in a network structure to simulate information processing, storage, and learning. The structure of an ANN usually consists of an input layer,

220 one or more hidden layers, and an output layer. The number of hidden layers determines the depth of an ANN (e.g. Schmidhuber, 2015, Hernández-Blanco et al., 2019). This structure is also known as the Multi-Layer Perceptron (MLP). The layers are composed of neurons in which the information processing takes place. Theoretically, the number of hidden layers and their neurons is unlimited. Thus, the network design is strongly dependent on the complexity and non-linearity of the task and the available processing capacity. Most ANNs utilized in LSA are feedforward networks, which have a multi-layer

225 perceptron (MLP) structure with usually one hidden layer (e.g., Ermini et al., 2005; Lee and Evangelista, 2006; Alimohammadlou et al., 2014).

The implemented module for artificial neural network (ANN) has an experimental status and runs comparable to the LR. ANN can utilize discrete and continuous data. Additionally, the user can specify the ANN properties. Among others, these settings comprise the number of neurons in the layers, the number of hidden layers, the activation function, and the solver to use. The

230 design of the network and the activation function selection is one of the most sensitive steps of the analysis with ANN. Despite reviewing numerous studies, we do not have a straightforward, practical recipe for designing the network yet. Therefore, the default settings do not represent the best practical approach but rather the defaults delivered with the *sklearn* library.

Nevertheless, the GUI and included data preprocessing provides easy and fast access to the capabilities given by the *sklearn* library and allow exploring the ANN performance for LSA. More technical information is obtainable from documentation of

235 LSAT PM and *sklearn* library.

The data scaling process runs identically to the LR module. After the training process, the output raster defining the spatial probability of landslide occurrence is exported to the corresponding result folder.

3.4.4 Analytical Hierarchy Process

As a heuristic approach, the AHP is different from the data-driven applications explained above. The user must specify the weights, usually based on his general expertise (knowledge of geological processes) and specific knowledge about the investigation area. The weighting process is a pairwise comparison of the inputs at different hierarchical levels. For LSA, the AHP typically takes two hierarchical levels. The first level controls the class priorities inside multiclass parameters (e.g., raster values), the second sets the priorities between the multiclass parameters (e.g., raster datasets).

The pairwise comparison is complex when working with parameters exhibiting many classes. The human's ability to compare is limited to approximately seven objects, plus or minus two (Miller, 1956). Saaty (1977) considered this proposing values between 1 and 9, specifying the factor's importance. Therefore, in the preparation process, it is advisable to reduce the number of classes by generalization or subdivision in different hierarchical groups (e.g., Balzer et al., 2020). The latter will make the hierarchy more complex.

The advantage of pairwise ranking compared to the simple ranking is the ability to verify the logical consistency of the decision mathematically. AHP uses the consistency ratio (CR) to indicate whether the introduced ranking is a logical inference or a random guess. Saaty (1980) recommends a CR under 0.1 for consistent assessment.

Notable is that some studies applying AHP for LSA use a hybrid approach combining bivariate methods with AHP (e.g., Kamp et al. 2008, 2010). In the hybrid approach, a data-driven bivariate approach applies to the first hierarchical level using, e.g., WoE. Afterward, additional expert-based weights derived from the AHP priority vector are applied to overlay the parameters to the model. Such an approach can preserve the crude generalization of the patterns in the first hierarchical level making the analysis applicable to more detailed datasets. For the AHP part, the method becomes more applicable by involving the expert weights at a higher hierarchical level, which benefits more from general process understanding than detailed local knowledge. Conversely, it also has implications for the bivariate analysis part. Using conditionally dependent parameters becomes less critical since experts adjust the parameter's contribution in the upper hierarchical level. However, the hybrid approach is only possible if a sufficient number of observations for the first data-driven step is available.

The implemented AHP is a pure expert-based tool supporting two hierarchy levels. The user has to perform the pairwise ranking for single parameter classes in the first step and the parameters in the second step.

3.5 Model Builder

The Model Builder (MB) is, in simple terms, a raster calculator with an integrated evaluation module. The algorithm behind the model evaluation is the receiver operating characteristics (ROC) curve - a technique to visualize and evaluate the classifier's performance (e.g., Fawcett 2006) by depicting the ratio of the True Positive Rate (Sensitivity) and the False Positive Rate (1-Specificity). The area under the ROC curve (AUC or AUROC) provides a quantitative measure to compare the goodness of different models.

At the start, MB automatically searches and imports analysis results and existing models to the corresponding weighted layer
270 and model collections, as shown in Fig. 3 (b and e). The user can specify which layers to include in the weighted overlay model shifting the layers into the model layer collection (Fig. 3c). The model generating expression is adjustable on demand. Default model generating expression is a simple additive overlay of selected weighted layers.

MB performs the overlay according to the data generating expression and uses the ROC curve to evaluate the model based on the specified landslide inventory dataset (Fig. 3a). Moreover, the evaluation procedure can be performed based on iterative
275 random subsampling or predefined sample groups. The user can select these options in the advanced settings of MB.

Using the training inventory, the user evaluates the model fit. For the test dataset, the user evaluates the predictivity of the model on new data. Using iterative subsampling, the user gets an idea about the variance of the model based on different samples that allows him to evaluate sampling errors (e.g., Torizin et al., 2018; Torizin et al., 2021). The latter might be a helpful feature for interpreting evaluation results if the test datasets are comparably small. Exploring the variance of the training
280 dataset in conjunction with the test ROC curve helps to understand whether the uncertainty of the model is the property of insufficient data (sampling error) or model accuracy (bias).

Moreover, the user can mix the model input layers (Fig. 3c) and adjust the generating expression (Fig. 3d). This flexibility allows the generation of hybrid models and model ensembles. Hybrid models combine different classifiers in one model, e.g., WoE for discrete data and LR for continuous data; model ensembles consist of different homogeneous models, e.g., LR and
285 ANN. Here it is essential to note that weighted layers or models generated by different classifiers may exhibit different value ranges and need transformations when used together in a hybrid model or model ensemble. Through the model building expression, the user can implement those transformations instantly.

MB's model collection (Fig. 3e) lists all generated models and provides essential management to export models to GeoTiff format and visualize the corresponding ROC curves (Fig. 3f). All generated models include metadata with information on
290 model input layers and applied model generating expression, making the results more reproducible. *Model Info* function provides access to the model's metadata.
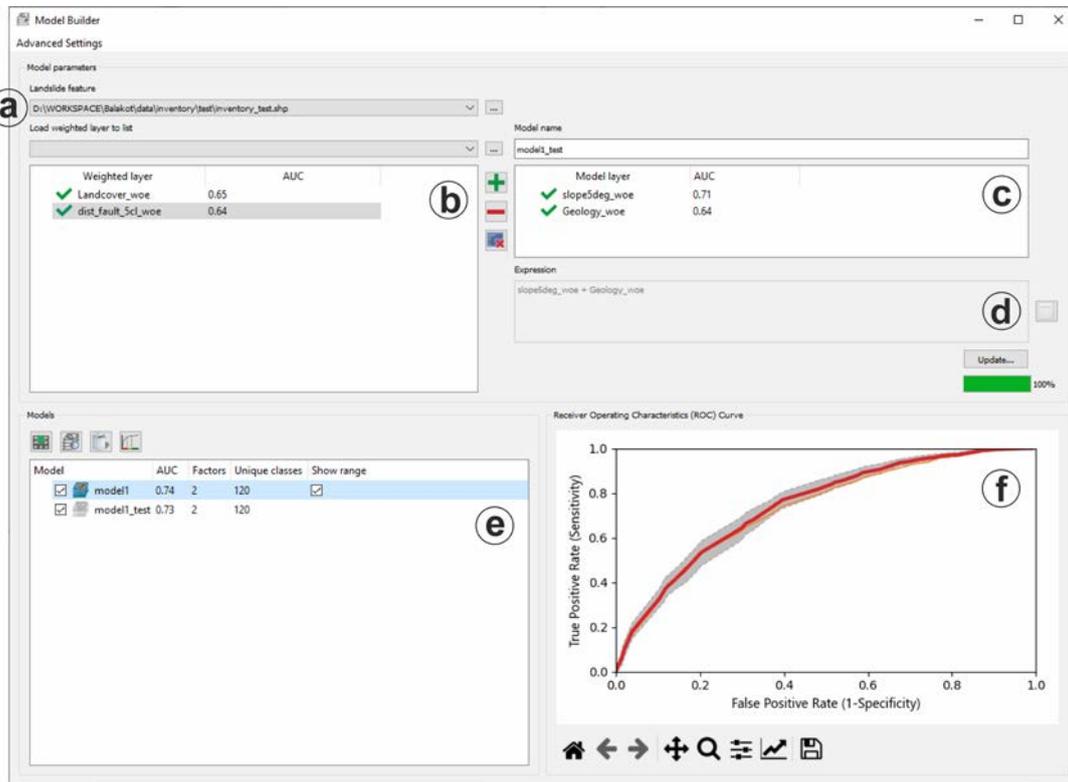
Figure 3: Model Builder GUI with its integral parts: a – Landslide inventory collection; b – weighted layer collection; c – model layer collection; d – model generating expression; e – models collection; f – ROC curves.

3.6 Zoning

The zoning procedure applies to all models generated or evaluated with LSAT PM. It uses the model's ROC curve to aggregate the model output with many different landslide susceptibility index (LSI) values to a legible map with few susceptibility zones. The zoning procedure follows the general concept proposed by Chung and Fabbri (2003). The basic idea is to specify class boundaries using cumulative landslide area over ranked unique condition classes representing the cumulative study area. Chung and Fabbri (2003) proposed to use the success rate depicting cumulative landslide area over the ranked cumulative area considered susceptible. However, it also partly applies to ROC curves since the y-axis representing the True Positive Rate corresponds to the cumulative landslide area. The x-axis in the ROC curve is the False Positive Rate depicting cumulative study area without landslide areas. In other words, areas that have been regarded as susceptible but do not contain landslide areas. Thus, the cumulative sum over the x-axis is only an approximation of the total study area, which is sufficiently accurate if the landslide areas are neglectable compared to the total area (e.g., when working with point data inventories in large regions). However, it also means that the accurate zone proportions cannot be directly estimated from the ROC curve graph if landslide areas are considerably large. Therefore, the *total area* values in the reclass table represent only approximations for zone area proportions.

Nevertheless, this discrepancy does not affect the implemented classification because we restrict the input to the proportion of
310   cumulative landslide areas within a zone. The specified cumulative landslide area value relates to the rank position of the
specific unique condition that exhibits a specific landslide susceptibility index (LSI). The LSI is finally used to set the
classification threshold for the class boundary. The zone areas in the attribute table of the output zoning raster are computed
directly from the raster values and represent accurate values. The other with success rate possible way to use the proportion of
the total area to specify an LS zone, e.g., 10% of the total area in the zone *Very high* is suppressed.
315   There are no well-established standards for the number of zones or the definition of zone boundaries. In our case studies (e.g.,
Torizin et al. 2017, Torizin et al. 2018), we used the proportions of 50% of all landslide pixels in the *Very high*, further 30%
for the *High*, 15% for the *Moderate*, 4% for the *Low* and about 1% for the V*ery low* susceptibility zone (Fig. 4). These
thresholds apply when the user selects the default table.

Alternatively, the user can use the *Reclassify* tool to aggregate the model to zones with customized thresholds directly on the
320   model's LSI or probability values.

Figure 4: Zoning tool with applied default classification.

4 Application example

4.1 Test data

325 A dataset to test the functionalities of the software is available from https://doi.org/10.5281/zenodo.5109620. The example or test dataset is an excerpt of the data collected in the German-Pakistani technical cooperation project Georisk Assessment Northern Pakistan (GANP), carried out by the Federal Institute for Geosciences and Natural Resources and Geological Survey of Pakistan (e.g., Torizin et al., 2017). The dataset covers about 664 square kilometers, including parts of the Kaghan and Siran Valleys in Khyber Pakhtunkhwa (KP), Northern Pakistan (Fig. 5a). Table 2 and Fig. 5 provide an overview of the test data.

330 **Table 2: Overview of the datasets in the test data.**

Data layer	Data Type	Source
Geology	raster, shapefile (.tif, .shp)	Calkins et al. (1975)
Landcover	raster, shapefile (.tif, .shp)	Fuchs et al. (2015)
AW3D30	raster (.tif)	JAXA (2017)
Confirmed faults	shapefile (.shp)	Calkins et al. (1975)
Landslides	shapefile (.shp)	Torizin et al. (2017)

A severe Kashmir Earthquake struck the region on 8 October 2005, with a moment magnitude of 7.8, triggering thousands of landslides. The collected landslide inventory results from the visual interpretation of optical satellite images available through Google Earth, which, during the data acquisition, consisted mainly of imagery from Quickbird (up to 0.60 m ground

335 resolution), IKONOS (~4 m ground resolution), SPOT (SPOT5 about 5 m ground resolution), and Landsat (15 m ground resolution) (Torizin et al., 2017). In total, the landslide inventory includes 3819 events for the test area depicted as polygons. Landslide sizes range from about 12 to about 88444 square meters representing the depletion area of the landslides (as far as it was possible to determine by visual interpretation of imagery).

The digital elevation model is the ALOS Global Digital Surface Model (AW3D30) (JAXA, 2017) with a ground resolution of

340 approximately 30 m (Fig. 5a). The geological information and the tectonic features (faults) were derived from the geological map of Calkins et al. (1975) (Fig. 5d and Tab. 3). The landcover results from the supervised classification on Landsat imagery performed by Fuchs et al. (2015) (Fig. 5c). The test dataset contains geology and landcover in raster and vector data formats. Note that the vector formats for parameters cannot be directly used for analysis in LSAT PM yet. However, the vector datasets may help test the *Vector Tools* (e.g., subsetting landslides based on specific geology or landcover class).

345
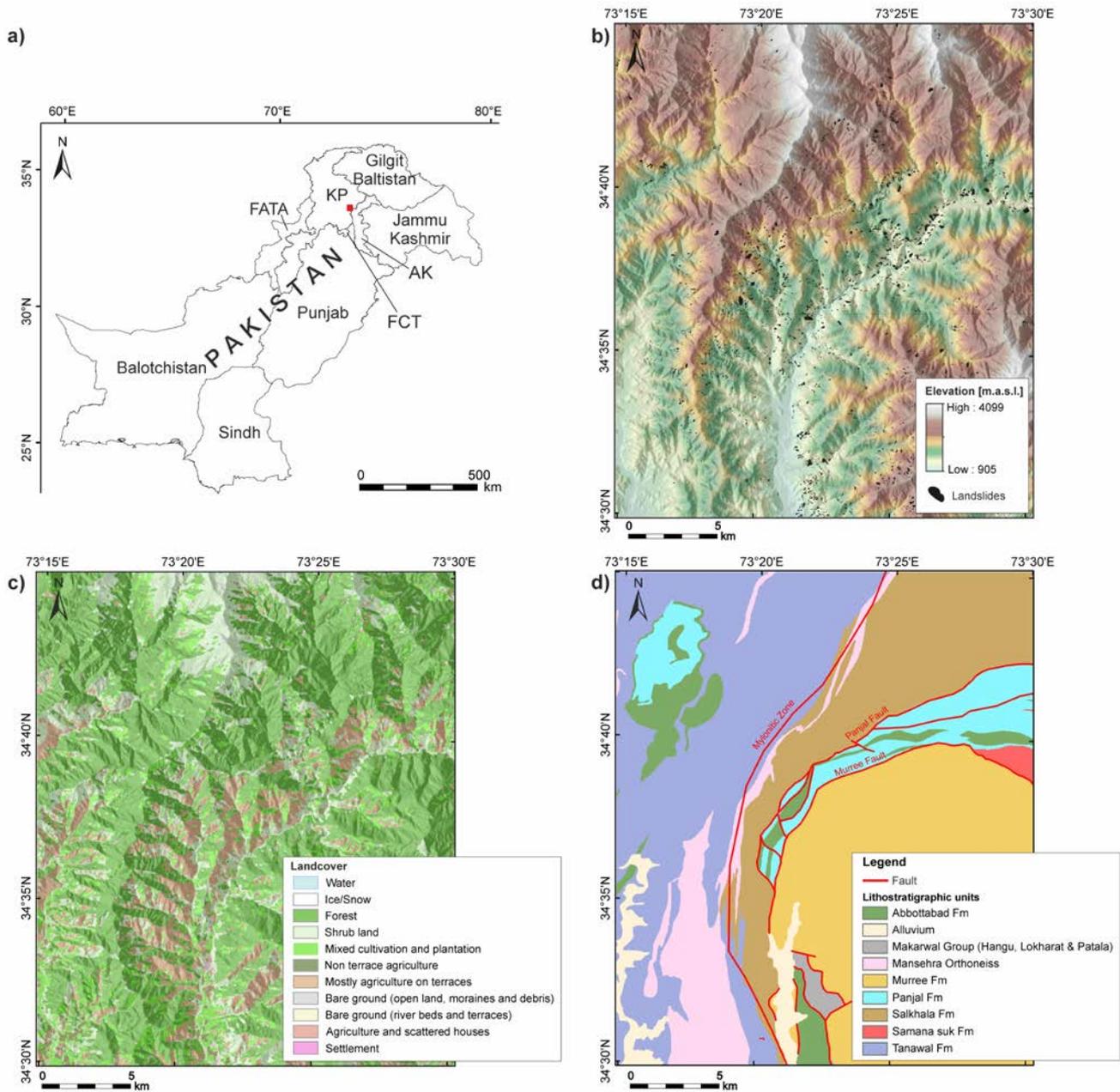
Figure 5: Example dataset. a) AW3D30 with landslide inventory; b) Landcover; c) Geology with prominent (confirmed) faults.

Table 3: Lithostratigraphic units of the geology layer with lithological description (after Calckins et al., 1975).

Lithostratigraphic unit	Lithological description
Abbottabad Fm	Dolomite, quartzite, phyllite, marble, and phosphate

Alluvium	Gravel, sand, silt, clay
Makarwal Group	Ferruginous oolitic sandstone, siltstone, and clay; massive nodular limestone with intercalations of marl and shales; shales and nodular limestone with coal seams
Mansehra Orthogneiss	Massive biotite granite, tourmaline-garnet granit gneiss and porphyroblastic granite gneiss
Murree Fm	Limestone and intercalated shales/marlstone
Panjal Fm	Carbonaceous slate, glassy quartzose, and agglomeratic sandstone
Salkhala Fm	Marble, graphite schist, quartz schist and qurtz-feildspathic gneiss
Samana suk Fm	Limestone and intercalated shales/marlstone
Tanawal Fm	Quartzose schist, quartzite, and schistose conglomerate

4.2 Analysis workflow

In the following example, we use the test dataset to showcase how to perform a simple LSA with WoE, LR, and ANN in LSAT PM and compare the model outputs. We skip the analysis with AHP in this example due to its high subjectivity and our lacking detailed knowledge about the investigation area.

Fig. 6 shows the principal workflow of the performed steps. The first seven steps cover the project creation, data import, and first preprocessing of the imported data, such as computation of the slope and euclidean distance and binning of continuous data in categories suitable for WoE. In step eight, the contingency analysis measures associations among discrete datasets based on Chi-square metrics. The utilization of strongly correlated datasets may lead to incorrect estimation of the factor's contribution and inflation of the estimated probability values (e.g., Agterberg and Cheng, 2002).

In step nine, we prepare the data to evaluate model uncertainties. Therefore, we compared the size of the landslide training and test datasets. In step two, the selected split option subdivided the imported landslide inventory into training containing 2674 events and the test dataset with 1146 events. The latter corresponds to approximately 43% of the training dataset. To estimate the sample size-dependent model variance, we generated 100 random subsamples from the training dataset the test dataset's size with the *Random sampling* tool. To make the results reproducible, we set the random seed to 42. The training and test inventory are random subsamples from the same dataset. Therefore, they represent the same spatial distribution but with a different mean sampling error (MSE) related to the sample size. Torizin et al. (2021) showed that evaluation of the model performance based on a test inventory of a smaller size than a training inventory must consider this for correct interpretation of the results. Evaluation with the 100 subsamples of the same size as the test inventory but derived from the training inventory dataset has two implications. First, all training events are known to the model and follow the same spatial distribution as the complete training inventory. Variations in model performance on these datasets define the MSE, which is expected to be in a

370 similar range by evaluating the model with a test dataset of the corresponding size. Thus, the shape of the ROC curve and AUC value should fall within the MSE range if the model generalizes well without significant overfit.
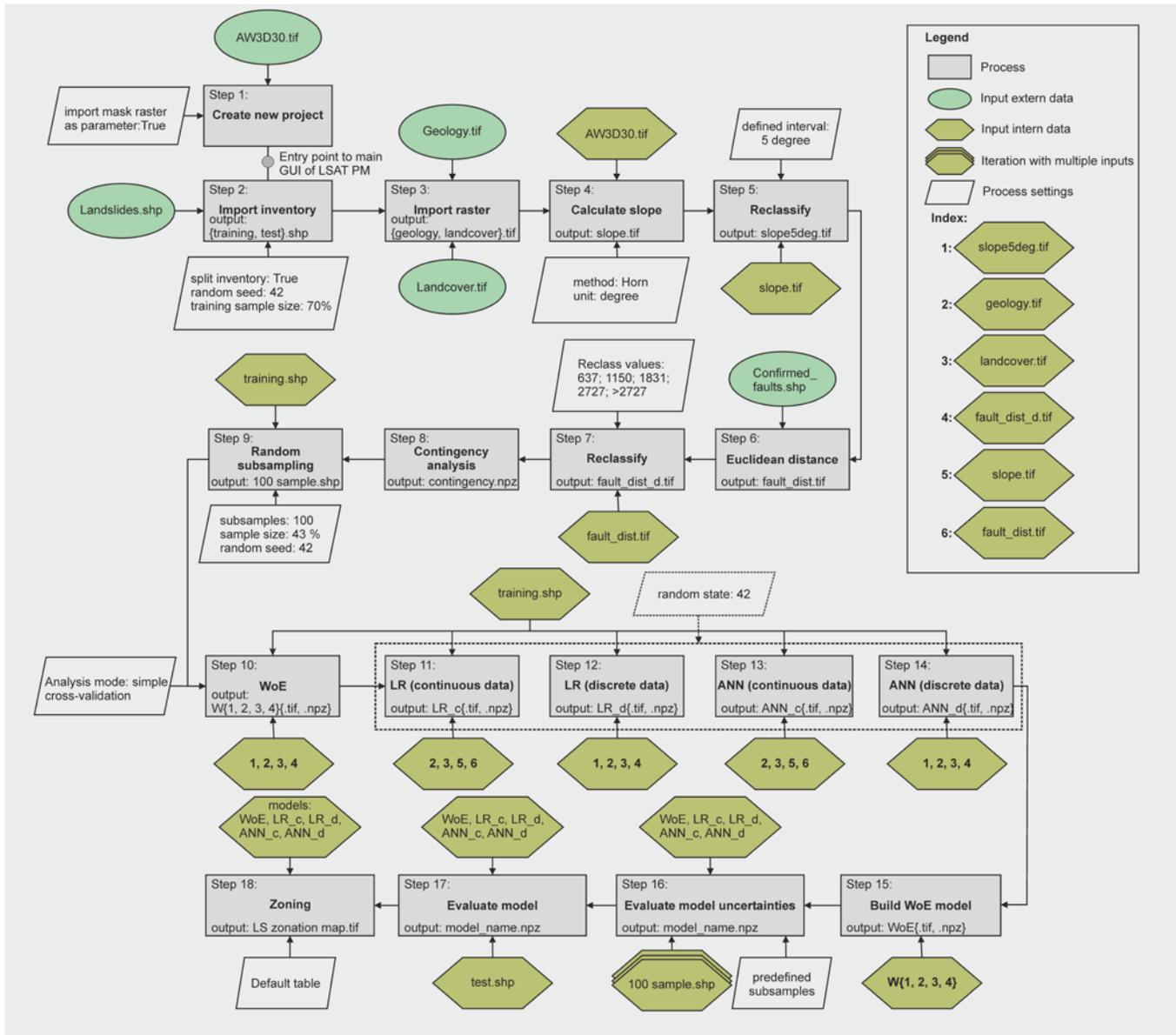
Figure 6: Workflow applied to the test dataset.

375 Steps 10 to 14 cover the analysis part. We calculated the WoE, LR, and ANN models in different ways to contrast the approaches. The WoE can utilize only discrete data; therefore, we used the classified and initially discrete data to generate the weighted layers. The LR and ANN support usage of both: continuous and discrete data. Therefore, we used the capability of

both approaches to utilize discrete and continuous data and generated two models for LR and ANN, respectively. The first marked with a _c suffix utilizes both data types, the second marked by _d suffix utilizes only discrete datasets as used in WoE.

Step 15 is the generation of the WoE model in MB by adding single weighted layers. To better compare the results from WoE with results from ANN and LR, we adjusted the model generating expression to transform the log-likelihoods of the WoE model into probabilities, applying the logistic function (see also Appendix A for details). In step 16, models uncertainties related to sampling error were evaluated in MB using 100 predefined subsamples generated in step nine. With this, the ROC curve is iteratively computed for every subsample. In the consecutive step, the models were evaluated with the test dataset not involved in the training process before, thus, representing new data. Finally, we used the ROC curve from the test dataset to generate legible susceptibility maps consisting of five susceptibility zones (default table, see Sect. 3.6) using the *Zoning tool*.

4.3 Results and discussion

While the first steps of data import and preparation, such as reclassing usual GIS functionalities, are trivial and are partially described in Sect. 3, the contingency analysis in step eight is worth examining. The results of the contingency analysis are saved in *NumPy* archive format (.npz) in the folder statistics.
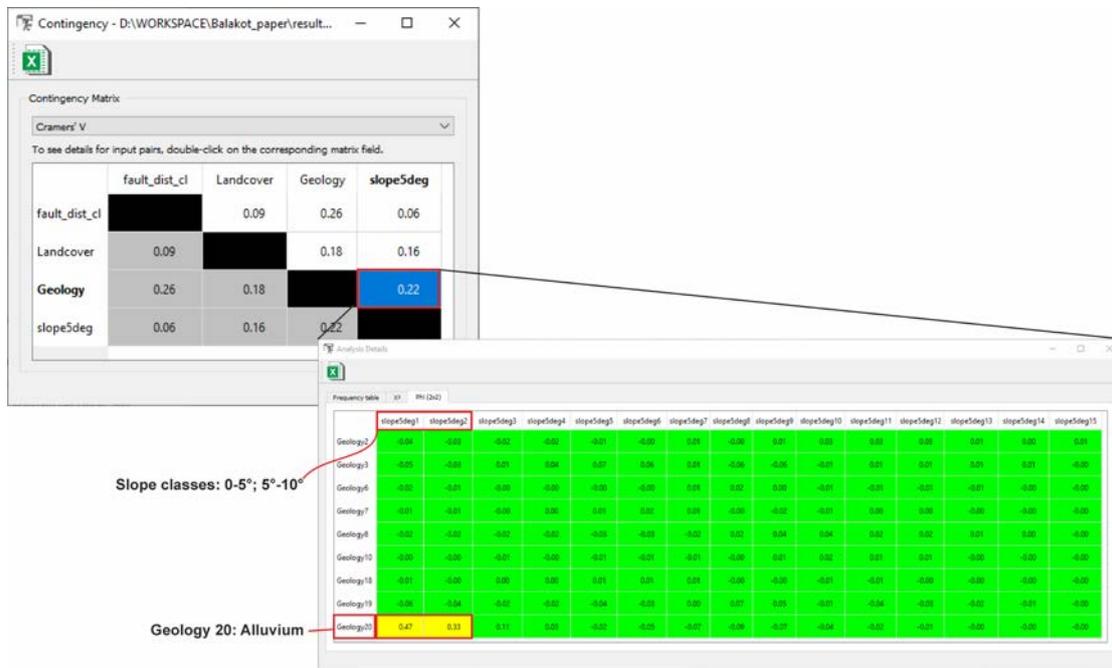
Figure 7 Example for the contingency result output: the first window represents an allover contingency matrix between multiclass parameters based on Cramer's V. On double-click, the detailed contingency between Geology and slope5deg is callable.

The analysis output consists of different tables (Fig. 7). The first result table shows the overview for all involved parameters based on Cramer's V and Pearsons C. Both metrics are estimates for the general association of the multiclass datasets. However, they do not allow to determine in detail whether, e.g., a moderate association comes from several moderately

associated classes or as an average estimate from one strongly associated class pair among others not correlated discrete classes. Therefore, an additional Phi metric based on the 2x2 contingency table is callable on double-click on the specific matrix cell, providing more detail for the specific parameter pair. It highlights the pairwise association among single variable class pairs.

400 The tables are colored to emphasize the strength of association: green for no to a marginal association, yellow for the moderate association, and red for the strong association. In Fig. 7, it is clear that while most classes of geology and classified slope layer are not correlated, a moderate association is present for alluvial deposits forming the valley fillings and slope between 0 and 10 degrees.

In the *WoE* tool, the user can explore the associations among the single factor and the occurrence of the events. The results

405 viewer contains all relevant information on the modeling process. The result table represents discrete class area distribution, corresponding landslide pixel frequencies in those classes, computed weights, variance, standard deviation, posterior probability values, and expected observations. The default output raster with suffix *_woe* derives from the table column *weights*. The included graphical representation of the results provides a quick overview of class and landslide pixel distributions, weights, and corresponding ROC curves (Fig. 8). WoE results can be exported as an analysis report in MS Word

410 format that concisely represents the relevant features.
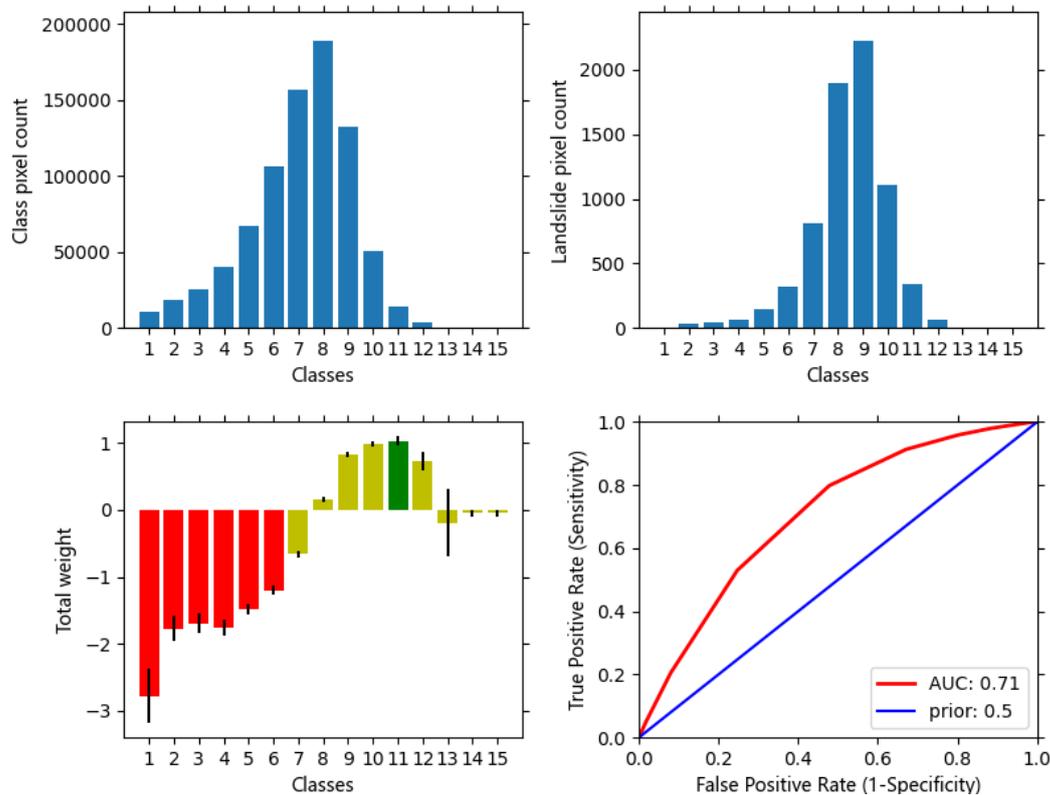
Figure 8 Graphical result output of WoE analysis for the simple-cross validation mode. Note that bar plots change to box or violin plots for other analysis modes such as, e.g., on-the-fly subsampling.

Outputs from LR and ANN analyses are compact. Among the involved parameters and model settings, LR results highlight the estimated coefficients and some informational metrics helping to find a tradeoff between model complexity (number of explanatory variables) and explained variance such as Akaike Information Criterion (AIC) and Bayesian Information Criterion (BIC), as well as the AUC of the corresponding ROC curve. The experimental ANN provides metadata on model inputs and settings, model score, and AUC value. For both, graphical result output and corresponding analysis reports are not implemented yet (see also Sect. 5).

The evaluation of model uncertainties in step 16 and model evaluation with test data in step 17 suggests that all three approaches deliver comparably good models. Although MB allows appropriate management for comparing the models (Fig. 9), we used customized scripts for the following figures 10, 11, and 13 (see Sect. 8) to showcase additional postprocessing possibilities based on LSAT PM outputs.
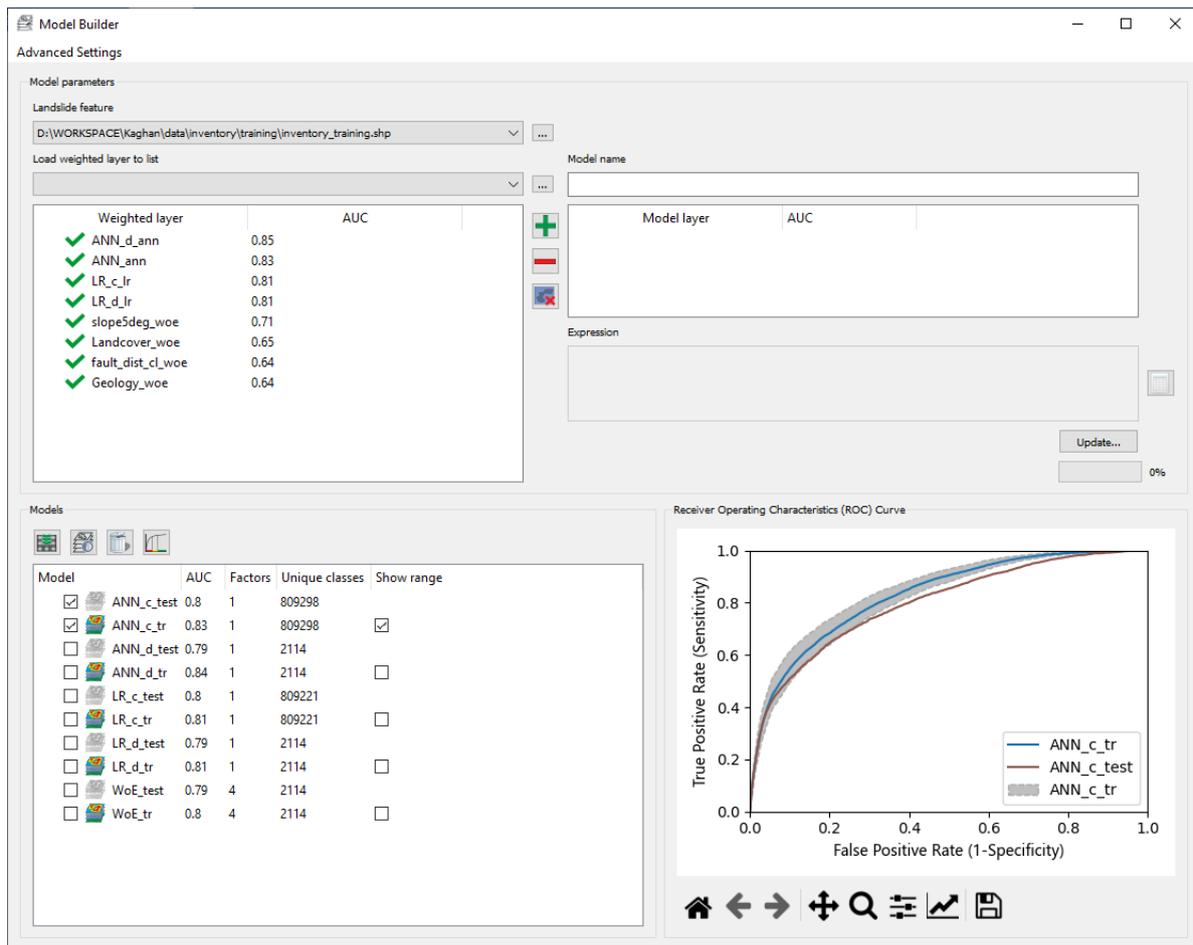
Figure 9 Evaluation and comparison of the models in MB.

To aggregate the results to a compact and legible figure (Fig. 10), providing some additional features not included in MB yet, we utilize the outputs of the MB. Figure 10 shows the performance of the models based on the predefined subsamples.
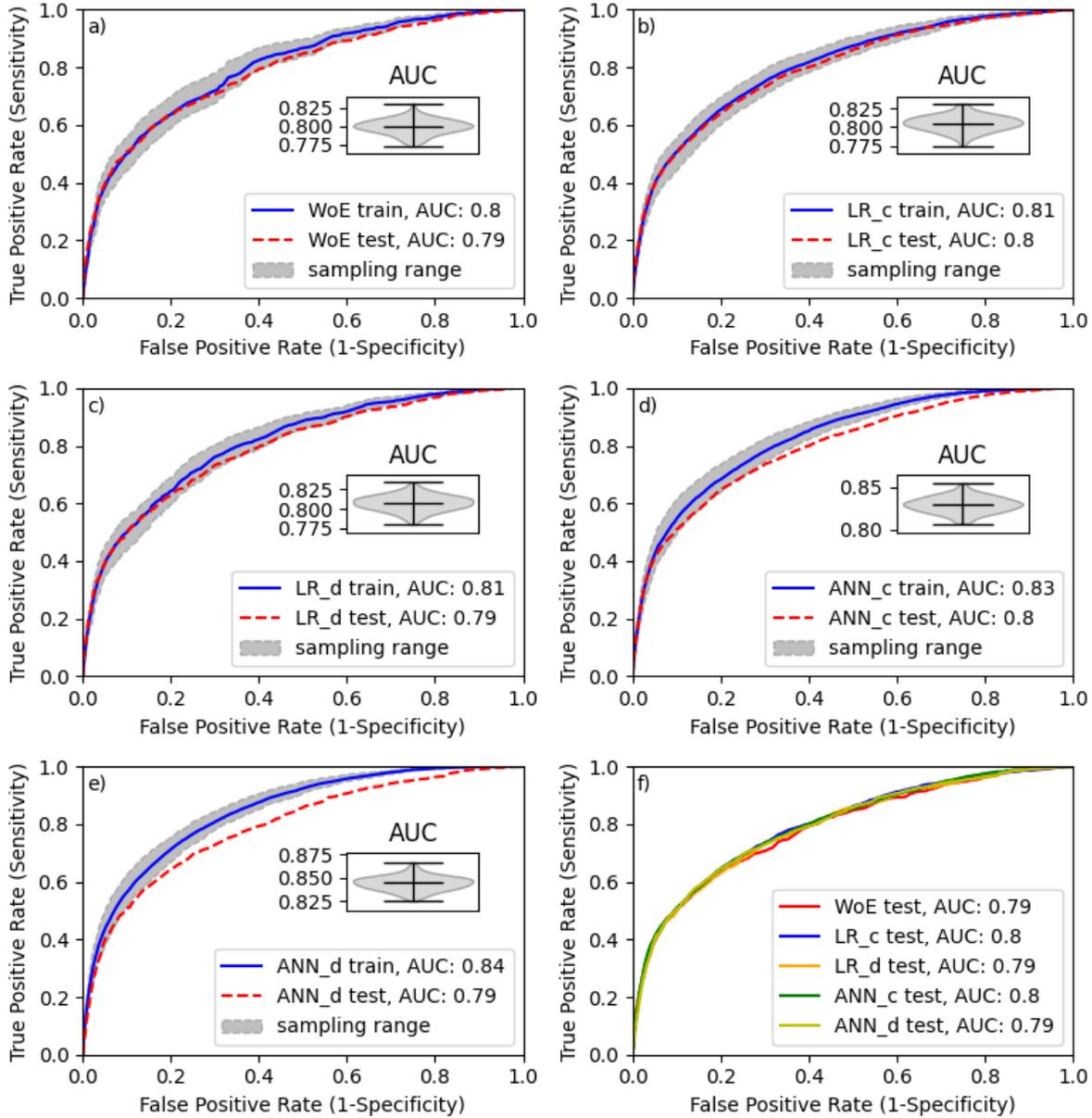
Figure 10 ROC curves for the different models. The greyish band marks the model uncertainty based on the MSE. The insert in a-e shows the corresponding distribution of AUC values for the utilized samples.

The greyish error band around the mean ROC curve indicates the MSE. As we can see from the violin plot inserts in Fig. 10a-e, the variance of the corresponding AUC values shows the normal distribution. At first glance, ANN_d and ANN_c models have the best training performance with AUCs of 0.84 and 0.83, followed by LR_c with an AUC of 0.81. WoE and LR_d model show the worst training performance (AUC of 0.80). For the model evaluation on test data, we see that for the WoE, LR_d, and LR_c, the test ROC curve is within the expected MSE. For ANN_c and ANN_d, however, the test performance is

significantly lower. In this case, we can interpret this as an overfit of the models. Using discrete variables in ANN_d, we introduced additional degrees of freedom compared to the ANN_c model; therefore, overfitting is more prominent in the ANN_d model. The reason is the flexibility of the ANNs with multiple neurons to fit also non-linear data relations, which might be an advantage but at the same time a significant uncertainty source. Thus, if we had aimed to optimize the susceptibility

440   map with ANN, we would need to review the network design or the number of iterations in the network training process to prevent overfitting. At this point, it is worth noting that imbalanced samples can also cause comparable effects. When using polygon landslide data, the imbalance may develop from rare large landslides appearing only in the training or the test inventory. Although this affects all model types, flexible ANN might suffer more than, e.g., WoE. The solution would be to check the distributions of the training and test landslide datasets and if imbalances are present to generate balanced samples

445   by, e.g., randomly drawing pixels from landslide areas instead of using them as a whole.

Because the interpretation of ANN results is not intuitive, we would generally recommend a parallel application of a multivariate linear model and ANN to see how much non-linearity is introduced by the ANN and how it affects the model generalization capabilities.

Further, looking at the test ROC curves of all models (Fig. 10f), we see that the predictivity of the models is comparable with

450   minor advantages for models utilizing continuous datasets. Thus, given the simple study design and available data, the models are equivalent alternatives from the statistical point of view. However, although the ROC curve provides a quantitative measure for classifier performance, as any statistical measure, it is not suitable for evaluating the model's reliability (e.g., Rossi et al., 2010). As we can demonstrate here, models with equivalent AUCs can exhibit substantially different susceptibility patterns. How meaningful those patterns are is beyond the statistical analysis capabilities and has to be verified based on other sources

455   of information.

We compare the susceptibility models in a pair plot to evaluate the differences in obtained susceptibility patterns. The pair plot in Fig. 11 visualizes the pairwise pixel-by-pixel comparison of the model values. The matrix diagonal shows the distribution of the model values (marginal probabilities). In contrast, the scatter plots in the lower matrix corner of Fig. 11 show the covariance of the value pairs overlain by linear regression to emphasize the trend. The pairwise comparison reveals general

460   linear relation for all models with better comparability for multivariate models ANN and LR but substantial differences in detail.
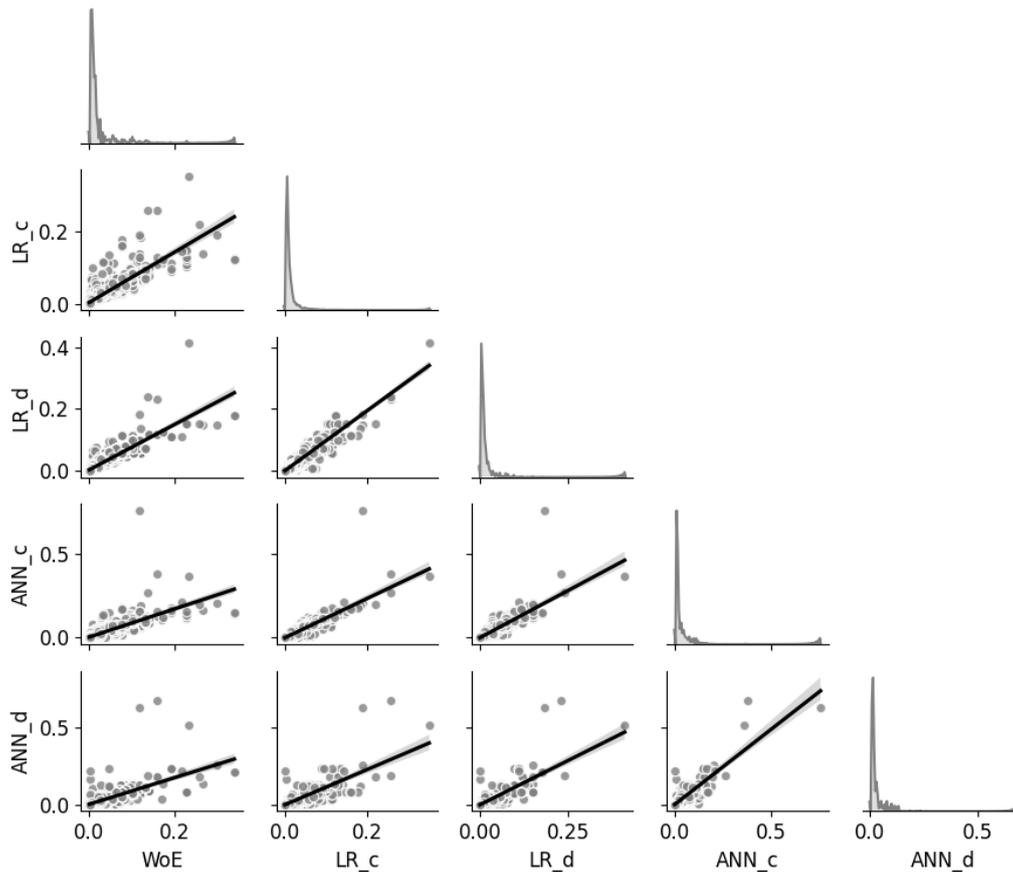
Figure 11 Pairwise comparison of the predicted landslide susceptibility patterns.

We wanted to see how these differences affect the final zonation and compared the models using simple class frequencies
465 statistics after the zonation procedure. Fig. 11 shows the landslide susceptibility maps after zonation with default values introduced in Sect. 3. In Fig. 12, the classified models are compared regarding their pixel counts within the susceptibility classes. While the highest susceptibility class containing 50% of all landslide pixels show minor differences, they become more significant in the lower susceptibility zones.
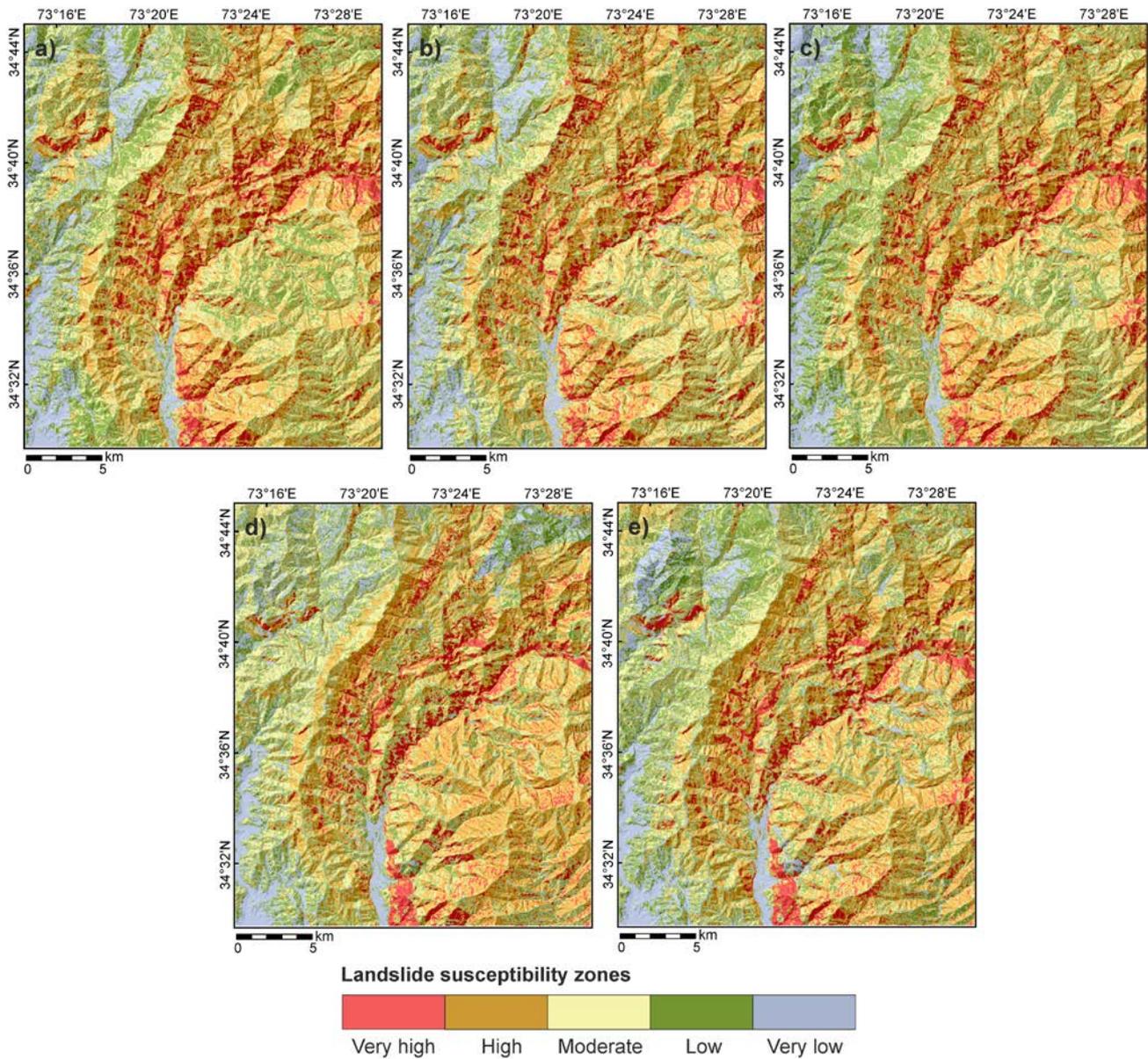
470 **Figure 12 Landslide susceptibility zones based on different models: a) WoE; b) LR_d; c) LR_c; d) ANN_d; e) ANN_c. *Very high* contains about 50%, *High* about 30%, *Moderate* about 15%, *Low* about 4% and *Very low* about 1% of all landslide pixels.**

	Very high	High	Moderate	Low	Very low
WoE	78583	259787	283331	124828	68733
LR_c	79679	244125	266754	162469	62235
LR_d	82373	247177	281848	118160	85704
ANN_c	76969	249599	252910	143732	92052
ANN_d	77879	260056	266404	125981	84942
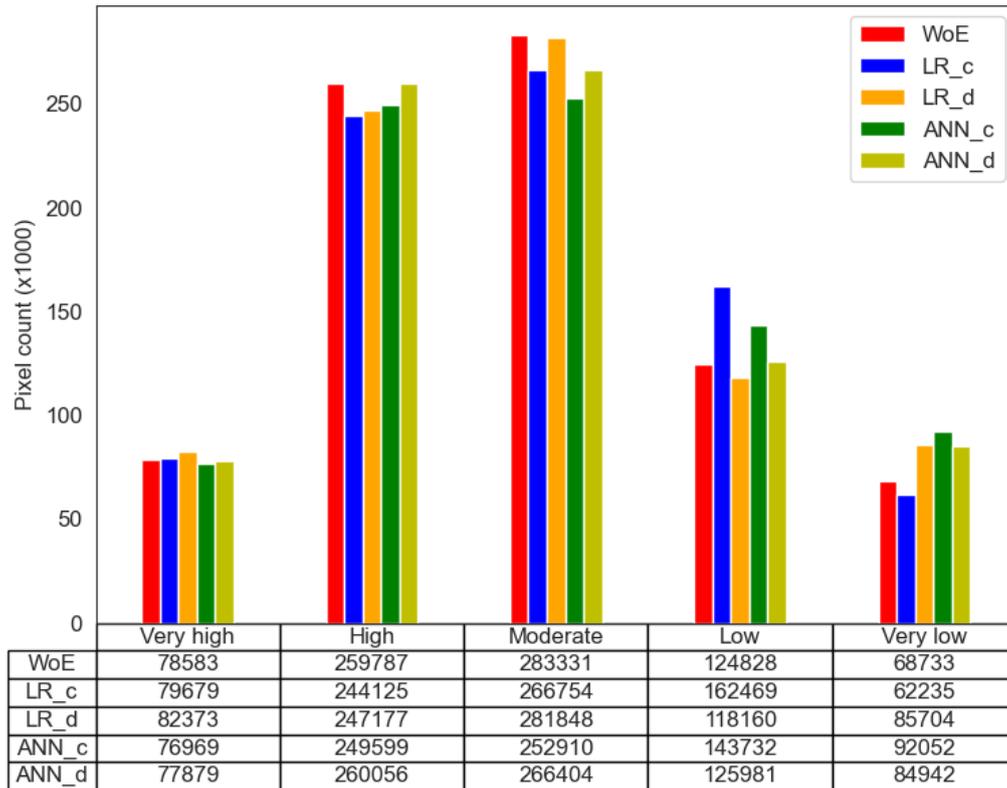
Figure 13 Susceptibility zones distribution for the susceptibility models. The values in columns show the number of pixels within the zones.

5 Conclusions and Outlook

In this paper, we introduced LSAT PM that provides a framework for applying and evaluating knowledge- and data-driven spatial binary classification methods and demonstrated in parts its capabilities based on a real-world test dataset. The given presentation is not exhaustive but provides a general idea of using the software.

Summarizing the capabilities of LSAT PM, we can emphasize that the project-based modular framework allows efficient data management at all steps of the LSA. The implemented logs on performed processing steps and metadata collection increase transparency and reproducibility and allow easy sharing of the modeling results, e.g., in working groups. At the same time, we tried to keep as many degrees of freedom as possible in the modeling procedures, providing the users not a fixed pipe but a toolkit that allows for flexible study designs. Thus, the preprocessing, analysis, and postprocessing steps are performable on the user's choice.

The MB module of LSAT PM implements functionalities allowing for practical evaluation of model uncertainties related to common sampling errors. Further, it provides a convenient way to compare models generated by the implemented algorithms and foreign models. The implemented raster calculator supports the generation of hybrid models and model ensembles.

LSAT PM targets a broad user profile. It provides access to LSA state-of-the-art methods to users beyond the academic community. Users with limited programming and scripting skills can perform analyses and explore the results via convenient GUI or export the results to other applications allowing further postprocessing. Skilled users can also benefit from implemented standards and quickly enhance the analysis outcomes stored in *NumPy* archive format by own scripts, as we have shown in Sect. 4. This versatility makes LSAT PM well suited for educational purposes at all levels.

Of course, there is always room for improvement. Therefore, the LSAT PM is subject to continuous further development. We intend to implement additional and improve existing methods, e.g., improve the AHP and machine learning workflows. Especially for the latter, we intend to implement additional features to visualize the results and increase the interpretability of the model outputs. We intend to implement GPU support to perform better on massive datasets in machine learning methods. Also, some management features such as a plugin builder tool that would support the easy implementation of customized plugins into the LSAT PM framework are under preparation. Software documentation continuously updates with the ongoing development and will be extended by short video tutorials introducing the work with LSAT PM.

With the open-source approach, we would like to encourage interested scientists to join the development, introducing and discussing new ideas and sharing experience in spatial modeling of landslides and scientific programming in general.

6 Appendices

Appendix A: Supporting Information for Weights of Evidence

WoE uses the Bayes rule to estimate the conditional probability of an event based on prior knowledge and a set of pieces of evidence. Prior knowledge in terms of prior probability usually represents the average expectation of an event given a study area. For the raster-based analysis, the prior probability calculates as the number of event pixels divided by the total pixels in the study area. Thus, the prior probability follows a uniform distribution over the entire study area (e.g., Torizin 2016). We update the prior probability by weighted evidence factors, which we assume to be conditionally independent. For the spatial analysis, the factors characterize how much the probability value in a specific location is higher or lower than the prior probability. The updated probability is called posterior probability (e.g., Teerarungsigul et al., 2015). The performed knowledge update cannot find new events but rather redistributes the probability density patterns conserving the total events (e.g., Agterberg and Cheng, 2002; Torizin, 2016). Thus, given the conditional independence of evidential patterns, we should obtain (approximately) the number of initial event pixels when summing up all pixels of the posterior probability raster. In practice, complete conditional independence of evidential patterns is seldom. Therefore, using many factors may cause inflation of posterior probability by occasional double counting of the effects (Agterberg and Cheng, 2002). The latter sets a general requirement to perform a contingency analysis (e.g., based on chi-square metrics) to estimate possible associations between evidence patterns.

In WoE, the weights for specific evidence patterns derive from the Bayes rule's formulation in logarithmic odds notation (e.g., Bonham-Carter et al., 1989; Bonham-Carter, 1994), considering the evidence as a binary pattern for presence or absence of a

520 specific feature. For multiclass datasets, the computation is done as if the dataset consists of several binary dummy variables. However, the straightforward analysis allows the weight calculation for multiclass datasets in one table without generating binary dummy variables explicitly. The weight calculation for a particular raster cell in a binary pattern distinguishes two cases. First, if the particular feature class *C* is present, then the logit is given by:

$$w^+ = log_e \left(\frac{P\{C|E\}}{P\{C|\bar{E}\}} \right). \tag{1}$$

525 else, the logit is given by:

$$w^- = log_e \left(\frac{P\{\bar{C}|E\}}{P\{\bar{C}|\bar{E}\}} \right). \tag{2}$$

where *P{C/E}* is the conditional probability of *C* (feature) given E (event); *P{C/Ē}* is the conditional probability of *C* given $\bar{E}$ (no event);

P{C̄/E} is the conditional probability of $\bar{C}$ (no feature) given *E; P{C̄/Ē}* is the conditional probability of $\bar{C}$ given $\bar{E}$.

530 The weight notations w^+ and w^- do not represent the mathematical sense of the values but the feature class presence (positive) and absence (negative) in the given raster cell.

With this formulation, positive logit values suggest a positive effect of the given variable, negative logits indicate a negative effect, and logits with a zero value indicate no effect. Thus, the latter does not modify the prior probability.

The posterior logit z is obtainable from weighted layers w_i (e.g., Barbieri and Cambuli, 2009; Torizin, 2016) as:

535 $$z = PriorLogit + \sum_{i=1}^{n} w_i. \tag{3}$$

where *n* is the number of weighted layers (evidence), and w_i is the *ith* weighted layer, and the *PriorLogit* is:

$$PriorLogit = log_e \left(\frac{\frac{\text{total landslide pixel}}{\text{total area pixel}}}{1 - \frac{\text{total landslide pixel}}{\text{total area pixel}}} \right). \tag{4}$$

To convert the logit formulation to posterior probability, we use the logistic function:

$$p_{post} = \frac{1}{1 + e^{-z}}. \tag{5}$$

540 The sum of the weighted layers from Eq. 3 is the default output in the LSAT PM model builder for WoE models. It is already sufficient to obtain the relative susceptibility pattern needed for evaluation. To obtain a model with probability values, the user should first compute the prior logit and modify the model generating expression in the model builder according to Eq. 5. Necessary information on the total number of landslide pixels and the total number of pixels in the study area is obtainable

from the result table of any weighted layer. We recommend exporting the result table to Excel and conducting the simple side calculation as shown in Eq. 4.

7 Code Availability

The current version of LSAT PM is available from the project website: https://github.com/BGR-EGHA/LSAT under the GNU GPL v3.0 license. The exact version of LSAT PM used to produce the results used in this paper is archived on Zenodo: https://doi.org/10.5281/zenodo.5909726. The LSAT PM documentation is available separately from https://github.com/BGR-EGHA/LSAT-Documentation under the CC BY-SA 4.0 license. The documentation for the exact version is archived on Zenodo: https://doi.org/10.5281/zenodo.5909744. The scripts used for postprocessing of the results in Sect. 4.3 are available from https://doi.org/10.5281/zenodo.5913626.

8 Data availability

The corresponding test dataset is archived on Zenodo: https://doi.org/10.5281/zenodo.5109620 under the CC BY-SA 4.0 license.

9 Author contribution

Jewgenij Torizin developed the theoretical concept and designed and coded LSAT PM. Nick Schüßler designed and coded parts of LSAT PM and migrated the code from Python 2.7 to Python 3. Michael Fuchs contributed with theoretical concepts and testing of the application through all stages of the development.

10 Competing interests

The authors declare that they have no conflict of interest.

11 Acknowledgements

We developed parts of the LSAT PM in the framework of a scientific-technical cooperation project between the Federal Institute for Geosciences and Natural Resources (BGR) and the China Geological Survey (CGS). This project was co-funded by the German Ministry of Economic Affairs and Energy (BMWi) and the Ministry of Natural Resources of the People's Republic of China. We also sincerely thank all colleagues who tested the prototypes of LSAT PM in its different development stages, helping us improve the software.

12 References

570   Agterberg, F. P., and Cheng, Q.: Conditional independence Test for Weight-of-Evidence Modeling. Natural Resources
        Research 11 (4): 249-255, https://doi.org/10.1023/A:1021193827501, 2002.

        Aleotti, P. and Chowdhury, R.: Landslide hazard assessment: summary review and new perspectives, Bull. Eng. Geol. Envir.,
        58(1), 21–44, https://doi.org/10.1007/s100640050066, 1999.

        Alimohammadlou, Y., Najafi, A., and Gokceoglu, C.: Estimation of rainfall-induced landslides using ANN and fuzzy
575   clustering methods: A case study in Saeen Slope, Azerbaijan province, Iran. Catena, 120, 149-162,
        https://doi.org/10.1016/j.catena.2014.04.009, 2014.

        Balzer, D., Dommaschk, P., Ehret, D., Fuchs, M., Glaser, S., Henscheid, S., Kuhn, D., Strauß, R., Torizin, J., Wiedenmann,
        J.: Massenbewegungen in Deutschland (MBiD) – Beiträge zur Modellierung der Hangrutschungsempfindlichkeit. Ein
        Kooperationsprojekt zwischen den Staatlichen Geologischen Diensten der Bundesländer Baden-Württemberg, Bayern,
580   Nordrhein-Westfalen, Sachsen und der Bundesanstalt für Geowissenschaften und Rohstoffe im Auftrag des Direktorenkreises
        der Staatlichen Geologischen Dienste in Deutschland. – Abschlussbericht, Augsburg, Freiberg, Freiburg, Hannover und
        Krefeld, 2020.

        Barbieri, G., Cambuli, P.: The weight of evidence statistical method in landslide susceptibility mapping 424 of the Rio Pardu
        Valley (Sardinia, Italy). 18th World IMACS/MODSIM Congress, Cairns, Australia, 2009.

585   Bonham-Carter, G. F., Agterberg, F. P. and Wright, D. F.: Weights of evidence modelling: a new approach to mapping mineral
        potential. Stat. Appl. Earth. Sci. Geol. Survey Can. Paper, 89–9, 171–183, 1989.

        Bonham-Carter, G. F.: Geographic information systems for geoscientists: Modelling with GIS. Ottawa: Pergamon Press, 1994.

        Bouziat, A., Schmitz, J., Deschamps, R., and Labat, K.: Digital transformation and geoscience education: New tools to learn,
        new skills to grow. European Geologist, 50, https://doi.org/10.5281/zenodo.4311379, 2020

590   Brabb, E. E.: Innovative approaches to landslide hazard and risk mapping. Proceedings of the 4th International Symposium on
        Landslides, Toronto, vol. 1, 307–324, 1985.

        Bragagnolo, L., da Silva, R. V., and Grzybowski, J. M. V.: Artificial neural network ensembles applied to the mapping of
        landslide susceptibility. Catena, 184, 104240, https://doi.org/10.1016/j.catena.2019.104240, 2020a.

        Bragagnolo, L., da Silva, R. V., and Grzybowski, J. M. V.: Landslide susceptibility mapping with r.landslide: A free open-
595   source GIS-integrated tool based on Artificial Neural Networks. Environmental Modelling & Software, 123, 104565,
        https://doi.org/10.1016/j.envsoft.2019.104565, 2020b.

        Brenning, A.: Statistical geocomputing combining R and SAGA: The example of landslide susceptibility analysis with
        generalized additive models. In J. Boehner, T. Blaschke and L. Montanarella (eds.), SAGA - Seconds Out (= Hamburger
        Beitraege zur Physischen Geographie und Landschaftsoekologie, vol. 19), 23-32, 2008.

600   Budimir, M. E. A., Atkinson, P. M., Lewis, H. G.:A systematic review of landslide probability mapping using logistic regression. Landslides, 12, 419–436, https://doi.org/10.1007/s10346-014-0550-5, 2015.

Buitinck, L., Louppe, G., Blondel, M., Pedregosa, F., Mueller, A., Grisel, O., Niculae, V., Prettenhofer, P., Gramfort, A., Grobler, J., Layton, R., VanderPlas, J., Joly, A., Holt, B., Varoquaux, G.: API design for machine learning software: experiences from the scikit-learn project, ECML PKDD Workshop: Languages for Data Mining and Machine Learning, 108-

605   122, 2013.

Calkins, J. A., Offield, T. W., Abdullah, S. K. M., Ali, T.: Geology of the Southern Himalaya in Hazara, Pakistan, and Adjacent Areas. Geological Survey Professional Paper 716-C, United States Government Printing Office, Washington, 1975.

Canny, S.: python-docx - A Python library for creating and updating Microsoft Word (.docx) files, retrieved on 4 May 2018 from https://pypi.org/project/python-docx.

610   Chung, C.-J., Fabbri, A. G.: Predicting landslides for risk analysis – Spatial models tested by a cross-validation technique, Geomorphology 94(3–4), 438-452, https://doi.org/10.1016/j.geomorph.2006.12.036, 2008.

Chung, C.-J., Fabbri, A. G.: Validation of spatial prediction models for landslide hazard mapping. Nat Hazards, 30, 451–472, 2003.

Crozier, M. J.: Deciphering the effect of climate change on landslide activity: A review. Geomorphology 124(3-4): 260-268.

615   https://doi.org/10.1016/j.geomorph.2010.04.009, 2010.

Ermini, L., Catani, F., and Casagli, N.: Artificial Neural Networks applied to landslide susceptibility assessment. Geomorphology, 66, 327-343, https://doi.org/10.1016/j.geomorph.2004.09.025, 2005.

Fawcett, T.: An introduction to ROC analysis. Pattern Recogn Lett, 27(8): 861–874. doi: 10.1016/j.patrec.2005.10.010, 2006.

Froude, M. J., Petley, D. N.: Global fatal landslide occurrence from 2004 to 2016. Nat. Hazards Earth Syst. Sci., 18: 2161–

620   2181. https://doi.org/10.5194/nhess-18-2161-2018, 2018.

Fuchs, M., Khalid N.: Land Cover Map for the Districts of Mansehra & Torghar, Province Khyber Pakhtunkhwa, Islamic Republic of Pakistan, Final Report, 44 p., Islamabad/Hannover, 2015.

Gazoni, E. and Clark, C.: openpyxl - A Python library to read/write Excel 2010 xlsx/xlsm files, retrieved on 11. June 2018 from https://openpyxl.readthedocs.io.

625   GDAL/OGR contributors: GDAL/OGR Geospatial Data Abstraction software Library. Open Source Geospatial Foundation. https://gdal.org, 2021.

George A. Miller: The Magical Number Seven, Plus or Minus Two: Some Limits on Our Capacity for Processing Information. The Psychological Review, 63, 81–97, https://doi.org/10.1037/h0043158, 1956.

GitHub Myanmar_Landslide_Models [code], https://github.com/katharineegan/Myanmar_Landslide_Models, last access: 17.

630   December 2021a.

GitHub Shallow landslide susceptibility analysis using Random Forest method in Val D''Aosta D'Aosta Valley [code], https://github.com/MattiaRaffa/RF-VDA-landslide-map, last access: 17. December 2021b.

GRASS Development Team: Geographic Resources Analysis Support System (GRASS) Software, Version 7.2.1 Open Source Geospatial Foundation. http://grass.osgeo.org, 2021.

635 Guzzetti, F., Carrara, A., Cardinali, M., Reichenbach, P.: Landslide hazard evaluation: a review of current techniques and their application in a multi-scale study, Central Italy. Geomorphology, 31:181-216. https://doi.org/10.1016/s0169-555x(99)00078-1, 1999.

Guzzetti, F., Reichenbach, P., Cardinali, M., Galli, M., Ardizzone, F.: Probabilistic landslide hazard assessment at the basin scale. Geomorphology, 72:272-299, https://doi.org/10.1016/j.geomorph.2005.06.002, 2005.

640 Hall-Wallace, M. K.: Integrating Computing Across a Geosciences Curriculum Through an Applications Course. Journal of Geoscience Education 47(2): 119-123, https://doi.org/10.5408/1089-9995-47.2.119, 1999.

Harris, C.R., Millman, K.J., van der Walt, S.J. et al.: Array programming with NumPy. Nature 585, 357–362, https://doi.org/10.1038/s41586-020-2649-2, 2020.

Hernández-Blanco, A., Herrera-Flores, B., Tomás, D., Navarro-Colorado, B.: A Systematic Review of Deep Learning
645 Approaches to Educational Data Mining. Complexity, Article ID 1306039, https://doi.org/10.1155/2019/1306039, 2019.

Hunter, J. D.: Matplotlib: A 2D graphics environment. Computing in Science & Engineering, 9(3), 90–95, https://doi.org/10.1109/MCSE.2007.55, 2007.

JAXA: ALOS Global DSM AW3D30 Dataset Product Format Description for V 1.1, available on http://www.eorc.jaxa.jp/ALOS/en/aw3d30/aw3d30v11_format_e.pdf, 2017.

650 Jebur, M. N., Pradhan, B., Shafri, H. Z. M., Yusoff, Z.M., Tehrany, M.S. An integrated user-friendly ArcMap tool for bivariate statistical modelling in geoscience applications. Geosci Model Dev 8:881–891. https://doi.org/10.5194/gmd-8-881-2015, 2015.

Kamp, U., Growley, B. J., Khattak, G. A., Owen, L. A.: GIS-based landslide susceptibility mapping for the 2005 Kashmir earthquake region. Geomorphology 101: 631-642, https://doi.org/10.1016/j.geomorph.2008.03.003, 2008.

655 Kamp, U., Owen, L. A., Growley, B. J., Khattak, G. A.: Back analysis of landslide susceptibility zonation mapping for the 2005 Kashmir earthquake: an assessment of the reliability of susceptibility zoning maps, Natural Hazards 54: 1-25, 2010.

Keefer, D. K.: Investigating Landslides Caused by Earthquakes – A Historical Review. Surveys in Geophysics, 23:473-510, https://doi.org/10.1023/A:1021274710840, 2002.

Lee, S., Evangelista, D. G.: Earthquake-induced landslide susceptibility mapping using an artificial neural network. Natural
660 Hazards and Earth System Sciences 6:687–695, https://doi.org/10.5194/nhess-6-687-2006, 2006.

Lee, S.: Application of logistic regression model and its validation for landslide susceptibility mapping using GIS and remote sensing data International Journal of Remote Sensing, 26:7, 1477-1491. https://doi.org/10.1080/01431160412331331012, 2005.

Lombardo, L., Mai, M. P.: Presenting logistic regression-based landslide susceptibility results. Engineering Geology 244: 14-
665 24, https://doi.org/10.1016/j.enggeo.2018.07.019, 2018.

Makkawi, M. H., Hariri, M. M., Ghaleb, A. R.: Computer Utilization in Teaching Earth Sciences: Experience of King Fahd University of Petroleum and Minerals. International Education Journal 4(2): 89-97, 2003.

Mathew, J., Jha V. K, Rawat, G. S.: Weights of evidence modelling for landslide hazard zonation mapping of Bhagirathi Valley, Uttarakhand. Current Science 92 (5): 628-638, 2007.

Merghadi, A.: An R Project for landslide susceptibility mapping in Mila basin (v1.1.0), Zenodo [code], https://doi.org/10.5281/zenodo.1000431, 2018.

Merghadi, A.: An R Project for landslide susceptibility mapping in Sihjhong basin, Taiwan (1.0.0), Zenodo [code], https://doi.org/10.5281/zenodo.3238689, 2019.

Moghaddam, M. H. R., Khayyam, M., Ahmadi, M., Farajzadeh, M.: Mapping susceptibility Landslide by using Weight-of Evidence Model: A case study in Merek Valley, Iran. Journal of Applied Sciences 7(22): 3342-3355, https://doi.org/10.3923/jas.2007.3342.3355, 2007.

Neuhäuser, B., Damm, B., Terhorst, B.: GIS-based assessment of landslide susceptibility on the base of the Weights-of-Evidence model. Landslides 9(4): 511-528, https://doi.org/10.1007/s10346-011-0305-5, 2012.

Osna, T., Sezer, E.A., Akgun, A.: GeoFIS: an integrated tool for the assessment of landslide susceptibility. Comput Geosci 66:20–30, https://doi.org/10.1016/j.cageo.2013.12.016, 2014.

Panchal, S., Shrivastava, A. K.: Application of analytic hierarchy process in landslide susceptibility mapping at regional scale in GIS environment. Journal of Statistics and Management Systems 23(2):199-206, https://doi.org/10.1080/09720510.2020.1724620, 2020.

Pedregosa, F., Varoquaux, G., Gramfort, A., Michel, V., Thirion, B., Grisel, O., Blondel, M., Prettenhofer, P., Weiss, R., Dubourg, V., Vanderplas, J., Passos, A., Cournapeau, D., Brucher, M., Perrot, M., Duchesnay, E.: Scikit-Learn: Machine Learning in Python. Journal of Machine Learning Research, 12, 2825-2830, 2011.

Petley, D. (2012) Global patterns of loss of life from landslides. Geology 40: 927–930, https://doi.org/10.1130/G33217.1.

Petschko, H., Brenning, A., Bell, R., Goetz, J., and Glade, T.: Assessing the quality of landslide susceptibility maps – case study Lower Austria, Nat. Hazards Earth Syst. Sci., 14, 95–118, https://doi.org/10.5194/nhess-14-95-2014, 2014.

Polat, A.: An innovative, fast method for landslide susceptibility mapping using GIS-based LSAT toolbox. Environ Earth Sci 80, 217, https://doi.org/10.1007/s12665-021-09511-y, 2021.

Polemio, M., Petrucci, O.: Rainfall as a Landslide Triggering Factor: an overview of recent international research. In Landslides in Research, Theory and Practice: Proceedings of the 8th International Symposium on Landslides; Bromhead, E., Dixon, N., Ibsen, M.-L., Eds.; Thomas Telford: London, UK, pp. 1219–1226, 2000.

Pradhan, B., Lee, S. (2010) Landslide susceptibility assessment, and factor effect analysis: back propagation artificial neural networks and their comparison with frequency ratio and bivariate logistic regression modelling. Environmental Modelling and Software 25: 747-759, https://doi.org/10.1016/j.envsoft.2009.10.016, 2010.

R Core Team: R: A language and environment for statistical computing. R Foundation for Statistical Computing, Vienna, Austria. ISBN 3-900051-07-0, http://www.R-project.org/, 2013

700   Reichenbach, P., Rossi, M., Malamud, B.D., Mihir, M., Guzzetti, F.: A review of statistically-based landslide susceptibility models. Earth Sci Rev 180: 60–91. https://doi.org/10.1016/j.earscirev.2018.03.001, 2018.

Rossi, M., Reichenbach, P.: LAND-SE: a software for statistically-based landslide susceptibility zonation, version 1.0. Geoscientific Model Development 9: 3533-3543, https://doi.org/10.5194/gmd-9-3533-2016, 2016.

Rossi, P. H., Guzzetti, F., Reichenbach, P., Mondini, A. C., Perruccacci, S.: Optimal landslide susceptibility zonation based

705   on multiple forecasts. Geomorphology, 114(3),129–142, https://doi.org/10.1016/j.geomorph.2009.06.020, 2010.

Saaty, T. L.: A scaling method for priorities in hierarchical structures. Journal of Mathematical Psychology 15: 234-281, 1977.

Saaty, T. L.: The analytic hierarchy process, New York: McGraw, 1980.

Sahin, E. K., Colkesen, I., Acmali, S. S., Akgun, A., Aydinoglu, A. C.: Developing comprehensive geocomputation tools for landslide susceptibility mapping: LSM tool pack. Computers & Geosciences,

710   104592, https://doi.org/10.1016/j.cageo.2020.104592, 2020.

Schmidhuber, J.: Deep Learning in neural networks: An overview. Neural Networks, 61, 85-117, 2015.

Senger, K., Betlem, P., Grundvåg, S-A., Horota, R., Buckley, S., Smyrak-Sikora, A., Jochmann, M., Birchall, T., Janocha, J., Ogata, K., Kuckero, L., Johannessen, R., Lecomte, I., Cohen, S., Olaussen, S.: Teaching with digital geology in the high Arctic: opportunities and challenges. 10.5194/gc-2021-6, 2021.

715   Tanyaş, H., Allstadt, K. E. and van Westen, C. J.: An updated method for estimating landslide-event magnitude. Earth surface processes and landforms, 43(9), 1836–1847, https://doi.org/10.1002/esp.4359, 2018.

Teerarungsigul, S., Torizin, J., Fuchs, M., et al.: An integrative approach for regional landslide susceptibility assessment using weight of evidence method: a case study of Yom River Basin, Phrae Province, Northern Thailand. Landslides. 13(5): 1151-1165, https://doi.org/10.1007/s10346-015-0659-1, 2015.

720   Tensor Flow Team: Abadi, M., Agarwal, A., Barham, P., Brevdo, E., Chen, Z., Citro, C., Corrado, G.S., Davis, A., Dean, J., Devin, M., Ghemawat, S., Goodfellow, I., Harp, A., Irving, G., Isard, M., Jozefowicz, R., Jia, Y., Kaiser, L., Kudlur, M., Levenberg, J., Mané, D., Schuster, M., Monga, R., Moore, S., Murray, D., Olah, C., Shlens, J., Steiner, B., Sutskever, I., Talwar, K., Tucker, P., Vanhoucke, V., Vasudevan, V., Viégas, F., Vinyals, O., Warden, P., Wattenberg, M., Wicke, M., Yu, Y., and Zheng X.: TensorFlow: Large-scale machine learning on heterogeneous systems. Software available from

725   tensorflow.org., 2015

Thiery, Y., Malet, J-P., Sterlacchini, S., Puissant, A., Maquaire, O.: Landslide susceptibility assessment by bivariate methods at large scales: Application to a complex mountainous environment. Geomorphology, 92(1-2), 38-59, ff10.1016/j.geomorph.2007.02.020, 2007.

Tian, T., Balzer, D., Wang, L., Torizin, J., Wan, L., Li, X., Chen, L., Li, A., Kuhn, D., Fuchs, M., Lege, T., Tong, B.: Landslide

730   hazard and risk assessment Lanzhou, province Gansu, China - Project introduction and outlook. In: Mikoš, M., Tiwari, B., Yin, Y., Sassa, K. (eds) Advancing culture of living with landslides, pp. 1027–1033. WLF 2017. Springer, Cham. https://doi.org/10.1007/978-3-319-53498-5_116, 2017.

Titti, G., Sarretta, A., Lombardo, L.: CNR-IRPI-Padova/SZ: SZ plugin (v1.0). Zenodo [code], https://doi.org/10.5281/zenodo.5693351, 2021.

735 Torizin, J., Fuchs, M., Awan, A. A., et al.: Statistical landslide susceptibility assessment of the Mansehra and Thorgar districts, Khyber Pakhtunkhwa Province, Pakistan. Natural Hazards 89(2): 757-784, https://doi.org/10.1007/s11069-017-2992-2, 2017.

Torizin, J., Fuchs, M., Balzer, D., Kuhn, D., Arifianti, Y., Kusnadi: Methods for generation and evaluation of landslide susceptibility maps: a case study of Lombok Island, Indonesia. Proceedings of 19th Conference on Engineering Geology, Munich, pp 253–258, 2013.

740 Torizin, J., Fuchs, M., Kuhn, D., Balzer, D., Wang, L.: Practical Accounting for Uncertainties in Data-Driven Landslide Susceptibility Models. Examples from the Lanzhou Case Study. In: Guzzetti F., Mihalić Arbanas S., Reichenbach P., Sassa K., Bobrowsky P.T., Takara K. (eds) Understanding and Reducing Landslide Disaster Risk. WLF 2020. ICL Contribution to Landslide Disaster Risk Reduction. Springer, Cham. https://doi.org/10.1007/978-3-030-60227-7_27, 2021.

Torizin, J., Wang, L. C., Fuchs, M., et al.: Statistical landslide susceptibility assessment in a dynamic environment: A case
745 study for Lanzhou City, Gansu Province, NW China. Journal of Mountain Science 15(6), https://doi.org/10.1007/s11629-017-4717-0, 2018.

Torizin, J.: Elimination of informational redundancy in the weight of evidence method: An application to landslide susceptibility assessment. Stochastic Environmental Research and Risk Assessment 30(2): 635-651, https://doi.org/10.1007/s00477-015-1077-6, 2016.

750 Torizin, J.: Landslide Susceptibility Assessment Tools for ArcGIS 10 and their Application. In: Proceedings of 34th IGC, Brisbane, 5-10 August 2012, p. 730, 2012.

Van Rossum, G., Drake, F. L.: Python 3 Reference Manual. Scotts Valley, CA: CreateSpace, 2009.

Van Westen, C. J., Castellanos Abella, E. A., & Sekhar, L. K.: Spatial data for landslide susceptibility, hazards and vulnerability assessment: an overview. Engineering Geology, 102(3-4), 112-131,
755 https://doi.org/10.1016/j.enggeo.2008.03.010, 2008.

Van Westen, C., Van Asch, T. W. and Soeters, R.: Landslide hazard and risk zonation – why is it still so difficult? Bulletin of Engineering Geology and the Environment, 65(2), 167–184, 2006.

Varnes, D. J.: Landslide hazard zonation: a review of principles and practice, Natural Hazards, 3. UNESCO. Paris. 63 pp., 1984.

760 Xu, Y., Goodacre, R.: On Splitting Training and Validation Set: A Comparative Study of Cross-Validation, Bootstrap and Systematic Sampling for Estimating the Generalization Performance of Supervised Learning. J. Anal. Test. 2, 249–262, https://doi.org/10.1007/s41664-018-0068-2, 2018.